Thermal Science and Engineering Progress 55 (2024) 102991

Contents lists available at ScienceDirect

Thermal Science and Engineering Progress

journal homepage: www.sciencedirect.com/journal/thermal-science-and-engineering-progress

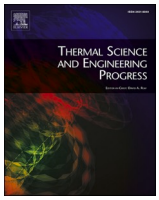

Enhancing building energy efficiency: Innovations in glazing systems utilizing solid-solid phase change materials

Hossein Arasteh [a,*], Wahid Maref [a], Hamed H. Saber [b]

[a] Department of Construction Engineering, École de Technologie Supérieure (ÉTS), University of Quebec, Montreal, QC H3C 1K3, Canada
[b] Deanship of Research and Industrial Development, and Mechanical Engineering Department at Jubail Industrial College, Royal Commission of Jubail and Yanbu, Jubail Industrial City 31961, Saudi Arabia

ARTICLE INFO

Keywords:
Building Energy
Solid-Solid Phase Change Material
Glazing System
Zero Energy Buildings
Computational Fluid Dynamics

ABSTRACT

This study investigates the energy efficiency of a double-glazing window (DGW) integrating a solid–solid phase change material (SSPCM) with limited thickness, applied to the inner glass pane within the air gap. Numerical model, validated against experimental data, is developed using a finite volume method in ANSYS Fluent. In this model, the Discrete Ordinates (DO) model is applied to simulate radiation, while the enthalpy-porosity approach is used to capture the solidification and melting processes in the phase change material. With this model, the energy performance of the system is analyzed under various transient temperature values (10 to 30 °C) and ranges (1 to 5 °C) during the coldest and hottest days of the year, as well as during cloudy and sunny days in Montreal (Dfb), Vancouver (Cfb), and Miami (Aw). According to the obtained results in Montreal, the DGW-SSPCM system consistently saves energy under summer sunny conditions, with optimal performance when the SSPCM remains transparent. However, it incurs energy losses in cloudy days, where the energy lost is 2.3 times greater than the energy saved in sunny days. In Vancouver, the system shows consistent energy savings, particularly at $T_c = 30$ °C, with average savings of 20.5 kJ (23 %) under summer sunny conditions. The system is most beneficial in Vancouver, where winter energy savings in cloudy days (50.6 kJ) are 7.1 times greater than the losses in sunny days (7.1 kJ). In Miami, the system results in energy losses by 60 % and 5 % (at $T_c = 30$ °C) under both summer sunny and cloudy conditions, respectively, indicating unsuitability for its climate. During winter sunny conditions, all three cities experience energy losses, with Vancouver showing the lowest of 7.1 kJ (3 %) and Montreal the highest of 64.4 kJ (19 %) at $T_c = 30$ °C. In winter cloudy conditions, the system saves energy in all cities, with the highest savings in Miami of 54.5 kJ (26 %) at $T_c = 30$ °C. Overall, the SSPCM-DGW system has proven to be beneficial in Vancouver across various conditions in terms of energy and visual performance. These findings highlight the necessity of considering localized climate factors when designing and implementing energy-efficient glazing systems. Finally, the SSPCM-DGW system has provided complete visual clarity during office hours, making it more suitable for commercial buildings.

1. Introduction

Building envelopes serve as the critical interface between indoor and outdoor environments, playing a significant role in mediating the conflicts between occupant comfort and the environmental impact of buildings. Adaptive facades, an advanced component of building envelopes, possess the ability to selectively transmit, filter, or block various phenomena such as heat, mass, and light. This capability enables them to regulate environmental conditions effectively, thereby enhancing indoor environmental quality. Additionally, adaptive facades offer a promising approach to reducing the energy consumption of buildings. By optimizing the interaction between the interior and exterior environments, adaptive facades contribute to improved indoor comfort and energy efficiency, ultimately supporting the development of more sustainable building practices. Among the opaque and transparent components of building envelopes, fenestration systems (e.g., windows, curtain walls, skylight devices) are identified as the primary source of heat loss in building constructions. These systems are responsible for approximately 60 % of the overall heat loss, significantly impacting the thermal efficiency of buildings [1].

There are three general methods to increase the thermal performance of glazing systems within buildings namely thermal resistance, solar control, and thermal inertia. The thermal resistance can be improved

* Corresponding author.
E-mail address: hossein.arasteh.1@ens.etsmtl.ca (H. Arasteh).

https://doi.org/10.1016/j.tsep.2024.102991
Received 11 June 2024; Received in revised form 9 October 2024; Accepted 14 October 2024
Available online 16 October 2024

Nomenclature

A	Area (m^2)
c_p	Specific heat (J/kgK)
d	Optical thickness (m)
h	Heat transfer coefficient (W/m^2K)
h_s	Sensible enthalpy (J/kg)
H	Enthalpy (J/kg)
ΔH	Latent heat (J/kg)
I	Radiation intensity (W/m^2)
k	Thermal Conductivity (W/mK)
L	Latent heat of fusion (kJ/kg)
n	refractive index
p	Pressure (Pa)
q''	Total heat flux (W/m^2)
$\vec{r}$	Position vector (m)
s	Sample thickness (path length) (m)
$\vec{s}$	Direction vector
$\vec{s}'$	Scattering direction vector
t	Time (s)
T	Temperature (°C)
T_c	Phase transition temperature (°C)
ΔT_c	Phase transition temperature range (°C)
v	Velocity (m/s)
$\vec{v}$	Velocity vector (m/s)

Greek symbols

β	Transparency fraction
μ	Dynamic viscosity (Pa s)
ρ	Density (kg/m^3)
σ_a	Absorption coefficient (1/m)
σ_s	Scattering coefficient (1/m)
τ	Transmittance
∅	Phase function
Ω'	Solid angle

Subscripts

op	Opaque
PCM	Phase change material
ref	Reference
tr	Transparent

Acronyms

DGW	Double-glazing window
PCM	Phase change material
SLPCM	solid–liquid phase change material
SSPCM	solid–solid phase change material

using different techniques such as the use of inert gases within the air gap of multi-glazing windows [2] as well as the use of materials with low thermal conductivity such as hydrogel [3] and aerogel [4]. To implement the second technique, solar control, different methods are available in literature such as photovoltaic systems [5], thermochromic [6] and thermotropic [7] materials, laminated coatings [8], low-e coatings [9], switchable systems [10], and so forth. The last approach in thermal performance enhancement of glazing systems, which is thermal inertia improvement and is the focus of current study, can be addressed by using thermal energy storage materials within the fenestration system like phase change materials (PCMs). The use of PCMs in glazing systems have been extensively reviewed in our recent research [11] showing a promising method in enhancing the thermal performance of glazing systems, however providing a satisfactory visual view has almost always been challenging. These materials absorb and release heat through phase change cycles, which can involve a solid-to-liquid transition, referred to as solid–liquid phase change material (SLPCM), or a solid-to-solid transition, known as solid–solid phase change material (SSPCM), as of the application within glazing systems. The current study implements the SSPCMs in glazing systems as they are advantageous compared to SLPCMs by offering low subcooling phenomenon, less material degradation, more consistent optical properties encapsulation-free implementation, no leakage, less phase-segregation, small volume variation, and high thermal stability [12]. Unlike SLPCMs, SSPCMs can be directly adhered to a surface or pane of a multi-glazing window with a specific thickness, remaining solid throughout their phase transition. This property allows the air or inert gas, which possesses low thermal conductivity, to remain between the indoor and outdoor environments. This arrangement is beneficial because SLPCM fills the air gap (connecting indoor and outdoor environments), it decreases the thermal resistance of the glazing system due to its higher thermal conductivity compared to air. Encapsulating SLPCM can mitigate this issue, allowing it to perform similarly to SSPCM by maintaining solid phase and preserving thermal resistance. SSPCMs undergo a phase transition between opaque (semi-crystalline) and transparent (amorphous) states, where only the soft segments melt, supported by the hard segment (polymeric backbone) with a significantly higher melting temperature. As a result, the SSPCM remains solid during phase transition by melting and freezing the soft segments, which are anchored by the hard segments. The phase transition process of SSPCMs has been comprehensively discussed and analyzed in [13,14], and [11].

Despite the extensive literature on SLPCM applications in glazing units, studies on SSPCMs in smart glazing are limited. Raj et al. [15] conducted a review study discussing the applications of SSPCMs and recent advancements in their thermophysical properties. This study compiled a comprehensive list of organic, polymeric, organometallic, and commercial SSPCMs, along with their thermophysical properties, phase transition temperatures, melting temperatures, molecular characteristics, and thermal behavior. These reviews serve as valuable resources for researchers and practitioners interested in utilizing SSPCMs in various applications. Another review study [12] focused on the molecular properties and thermal characteristics of SSPCMs for thermal energy storage. They examined the relationship between molecular structure, phase transition mechanisms, and thermal properties of the four main categories of SSPCMs: polymeric, organic, organometallic, and inorganic. The authors provided guidance on selecting appropriate SSPCMs for various applications based on desired physical, thermal, and mechanical properties, offering a comprehensive list within each main category. Guldentops et al. [16] explored a building enclosure system utilizing SSPCMs to passively regulate temperature in a south-facing building in central Massachusetts, accounting for both summer and winter climates. They developed a finite element model to analyze the system's energy performance, identifying optimized configurations for each season. However, the study noted the need for refining the extinction coefficients and transition temperatures of SSPCMs for effective year-round operation. Gao et al. [13] integrated a thin SSPCM layer into the interior side of a double-glazing window (DGW) and performed a numerical analysis to evaluate annual energy savings. The authors used EnergyPlus for the numerical study but had to develop an equivalent model due to the software's limitations in simulating latent energy storage materials. The results showed that a 3 mm SSPCM layer improved energy savings in warm, mixed, and cold climates, surpassing the performance of low-emissivity windows. Ma et al. [17] assessed a glazing system combining silica aerogel and SSPCM in a severe cold region of China, focusing on both daylighting and energy performance. EnergyPlus was used for energy analysis, and Radiance software for

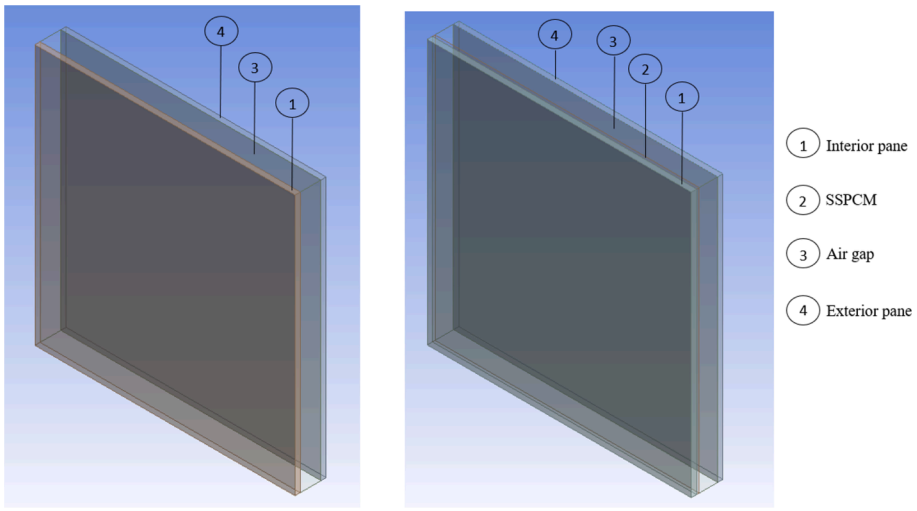

Fig.1. The 3D geometry of (a) DGW-REF and (b) DGW-SSPCM.

Table 1
Thermophysical properties of the used materials.

	Density (kg/m^3)	Specific heat (J/kgK)	Thermal conductivity (W/mK)	Absorption coefficient (1/m)	Scattering coefficient (1/m)	Refractive index	Latent heat (kJ/kg)
Air*	1.225	1006.43	0.0242	0	0	1	–
Glass [20]	140	840	1.3	19	0	1.5	–
SSPCM [21]	1055	1630	0.36	33.80 (transparent) 25.73 (opaque)	0 (transparent) 119.02 (opaque)	1.11 (transparent) 5.33 (opaque)	110

*Properties at temperature range 10∼30°C[22].

daylighting analysis. Similar to Gao et al. [13], due to software limitations, an equivalent SSPCM model was employed. The study identified transition temperature, latent heat, absorption coefficient, and refractive index as key parameters through sensitivity analysis. A 10 mm thickness of silica aerogel was recommended to maximize energy savings while meeting daylighting standards in China. Their findings suggested the viability of employing DGW-SSPCM in severe cold regions. Wang et al. [14] developed an inverse model to derive expressions for the extinction coefficient and refractive index of SSPCMs as a function of temperature for the translucent phase, providing constant values for the opaque and transparent phases. These optical properties were incorporated into the current study. Recently, Zhang et al. [18] conducted a two-dimensional numerical parametric study using the finite volume method to investigate the optical and thermal properties of a triple-glazed window containing SSPCM in the inner air gap and silica aerogel in the outer air gap. The study simulated 24 h of severe cold weather in a Chinese city. Sensitivity analysis indicated that the thermal efficiency of the glazing system was significantly affected by the melting temperature and latent heat of the PCM, with the absorption coefficient and refractive index having minor effects. The optimal melting temperature of the PCM was found to be 18 °C, resulting in a 15 % energy saving rate.

Based on the aforementioned literature review, it is evident that there are few studies investigating the energy performance of SSPCMs in glazing systems using 3D modeling. The existing numerical models are either using EnergyPlus that has some limitations in capturing the phase transition phenomenon within the SSPCM, hence using an equivalent model has been inevitable or 2D models that assess the SSPCM behavior fully filled the air gap space of a triple-glazed window. Therefore, to bridge this gap, the main objective of this study is to develop a 3D model and use it to assess the energy performance of a DGW incorporating SSPCMs. The idea of placing the SSPCM onto the interior pane between the air gap has come up to keep the material's temperature as high as possible to yield an almost full transparent window throughout the whole year. Following model validation, a parametric study was conducted by varying the transient temperature and transient temperature range of a south-facing DGW-SSPCM over a 24-hour real-time period. The simulations were performed for sunny and cloudy days during the coldest and hottest days of the year 2022 in Montreal, Vancouver, and Miami.

2. Methodology

2.1. Geometrical details

In the current study the results of a double-glazing window integrated with a solid–solid phase change material (DGW-SSPCM) is compared to a reference double-glazing window (DGW-REF). The SSPCM has been adhered to the interior pane of the DGW within the air gap. Both DGW-REF and DGW-SSPCM consist of two panes, each measuring 20 cm in length, 20 cm in width, and 4 mm in thickness. The DGW-REF configuration features a 1.6 cm air gap, shown in Fig. 1a. In contrast, the DGW-SSPCM configuration incorporates a 2 mm-thick SSPCM layer on the interior pane, reducing the air gap to 1.4 cm, shown in Fig. 1b.

2.2. Material perspective

In the current study, the glazing system is composed of two 4 mm clear glass with an emissivity of 0.9 [19]. The thermophysical and

Table 2
List of studied scenarios in this study.

Summer	cases	Glazing system	Winter	cases	Glazing system
	0	DGW-REF		0	DGW-REF
	1	$T_c = 20^{\circ}C, \Delta T_c = 1^{\circ}C$		1	$T_c = 10^{\circ}C, \Delta T_c = 1^{\circ}C$
	2	$T_c = 20°C, \Delta T_c = 3°C$		2	$T_c = 10°C, \Delta T_c = 3°C$
	3	$T_c = 20°C, \Delta T_c = 5°C$		3	$T_c = 10°C, \Delta T_c = 5°C$
	4	$T_c = 25°C, \Delta T_c = 1°C$		4	$T_c = 15°C, \Delta T_c = 1°C$
	5	$T_c = 25°C, \Delta T_c = 3°C$		5	$T_c = 15°C, \Delta T_c = 3°C$
	6	$T_c = 25°C, \Delta T_c = 5°C$		6	$T_c = 15°C, \Delta T_c = 5°C$
	7	$T_c = 30°C, \Delta T_c = 1°C$		7	$T_c = 20°C, \Delta T_c = 1°C$
	8	$T_c = 30°C, \Delta T_c = 3°C$		8	$T_c = 20°C, \Delta T_c = 3°C$
	9	$T_c = 30°C, \Delta T_c = 5°C$		9	$T_c = 20°C, \Delta T_c = 5°C$

optical properties were obtained from [20]. The thermal energy storage material (SSPCM) was chosen from [21]. The optical properties of the SSPCM including refractive index as well as absorption and scattering coefficients were derived from correlations developed by [14]. The thermophysical properties of the materials employed in this study are detailed in Table 1. Additionally, Table 2 lists the various phase change temperatures and their respective ranges that were examined in this research.

The optical thickness (d) of a substance, defined by Eq. (1), is a common way to describe the extinction coefficient [22]. In this equation, s refers to the sample's actual thickness, which is specified as 2 mm for the SSPCM-DGW setups in this study.

$$d = (\sigma_{a+}\sigma_s)s \tag{1}$$

In Equation (1), σ_a and σ_s represents the absorption and scattering coefficients, respectively. This study assumes an isotropic scattering coefficient. By applying Beer-Lambert's law to non-gaseous materials, Eq. (2) can be used to calculate the PCM transmittance [16]:

$$\tau_{PCM} = 10^{-d} \tag{2}$$

where τ_{PCM} represents the transmittance of the PCM. First, the absorption coefficient is calculated using Eq. (3) [20]. This value is then applied in Eq. (1) to determine the scattering coefficient.

$$\sigma_a = \sigma_s\left[\frac{\tau_{PCM,tr} - \tau_{PCM,op}}{1 - \tau_{PCM,op}}\beta + \frac{1 - \tau_{PCM,tr}}{1 - \tau_{PCM,op}}\right] \tag{3}$$

In Equations (1) to (3), τ and β represent the transmittance and transparency fraction of the material, respectively. The subscripts PCM, tr, and op represent the phase change material, transparent and opaque, respectively. For the SSPCM, the refractive index and extinction coefficient are as follows: for the transparent phase, they are 1.11 and 25.73 m^{-1}, respectively, and for the opaque phase, they are 5.33 and 152.82 m^{-1}, respectively [14]. For the translucent phase, Eqs. (4) and (5) are used to calculate the average optical properties as a function of the transparency fraction, which replaces the term 'liquid fraction' since there is no liquid phase in SSPCM. The transparency fraction represents the portion of the material in the transparent phase, with β being 0 for fully opaque SSPCM and 1 for fully transparent SSPCM. When the transparency fraction is 0, it indicates that the SSPCM temperature is at or below the lower limit of the transient temperature range, known as the opaqueus temperature (akin to liquidus temperature in SLPCM), meaning the material is in the opaque phase. Conversely, a transparency fraction of 1 indicates that the SSPCM temperature is at or above the upper limit of the transient temperature range, known as the transparentus temperature (akin to solidus temperature in SLPCM), meaning the material is in the transparent phase. A transparency fraction between 0 and 1 signifies that the SSPCM is in the translucent phase, similar to the mushy zone in SLPCMs.

$$\sigma_{a,cell} = 33.8\beta + 25.73(1-\beta) \tag{4}$$

$$\sigma_{s,cell} = 119.02(1-\beta) \tag{5}$$

2.3. Governing equations

To model the SSPCM, the enthalpy-porosity approach in FLUENT was utilized, assigning a very high viscosity value to the SSPCM to ensure nearly zero velocity within it. In this study, natural convection effects within the air gap of the DGW were neglected for all configurations (i.e., DGW-SSPCM and DGW-REF) to focus on evaluating the feasibility and effectiveness of incorporating SSPCM into glazing systems. Using the climate in three cities with different climatic conditions (i.e. Montreal, Vancouver, and Miami) as a case study under natural conditions, this approach aims to determine whether energy savings can be realized in a glazing system with SSPCM compared to one without it. The governing equations for this study considering the Discrete Ordinates (DO) model for radiation and a solidification/melting model for SSPCM are as follows.

- Mass conservation equation [22]:

$$\frac{\partial \rho}{\partial t} + \nabla.(\rho\vec{v}) = 0 \tag{6}$$

- Momentum conservation equation [22]:

$$\frac{\partial}{\partial t}(\rho\vec{v}) + \nabla.(\rho\vec{v}\vec{v}) = -\nabla \mathrm{p} + \nabla.(\mu\nabla\vec{v}) + S_m\vec{v} \tag{7}$$

In Equations (6) and (7), ρ, t, $\vec{v}$, p, and μ are density, time, velocity vector, pressure, and dynamic viscosity, respectively. It is noteworthy to mention that, the source term "$S_m\vec{v}$" should be added to the right-hand side of Equation (7) according to the solidification/melting modeling. S_m is defined as the negative of the porosity function ($A_m(\beta)$), as described by Brent et al. [23]. The porosity function is formulated in order to make the momentum equations behave the Carman-Kozeny equations [24], which are used to describe fluid flow in porous media. However, this study employs an SSPCM, which lacks internal fluid flow, rendering the source term ineffective in the momentum equations.

- Energy equation [22]:

$$\frac{\partial}{\partial t}(\rho H) + \nabla.(\rho\vec{v}H) = \nabla.(k\nabla \mathrm{T}) + \mathrm{S}_h \tag{8}$$

In Eq. (8), the enthalpy of the PCM, H, is calculated as the sum of the sensible enthalpy, h_s, and latent heat, ΔH as:

$$H = h_s + \Delta H \tag{9}$$

where,

$$h_s = h_{s,ref} + \int_{T_{ref}}^{T} c_p dT \tag{10}$$

In Eq. (9), the fractional latent heat of the PCM, ΔH, can be expressed in terms of the PCM's latent heat of fusion, L. Note that ΔH can vary between 0 (opaque phase), L (transparent phase), and values between 0 and L when $T_{opaqueus} < T < T_{transparentus}$ (translucent phase).

$$\Delta H = \beta L \tag{11}$$

In this study, the transparency fraction is calculated as following:

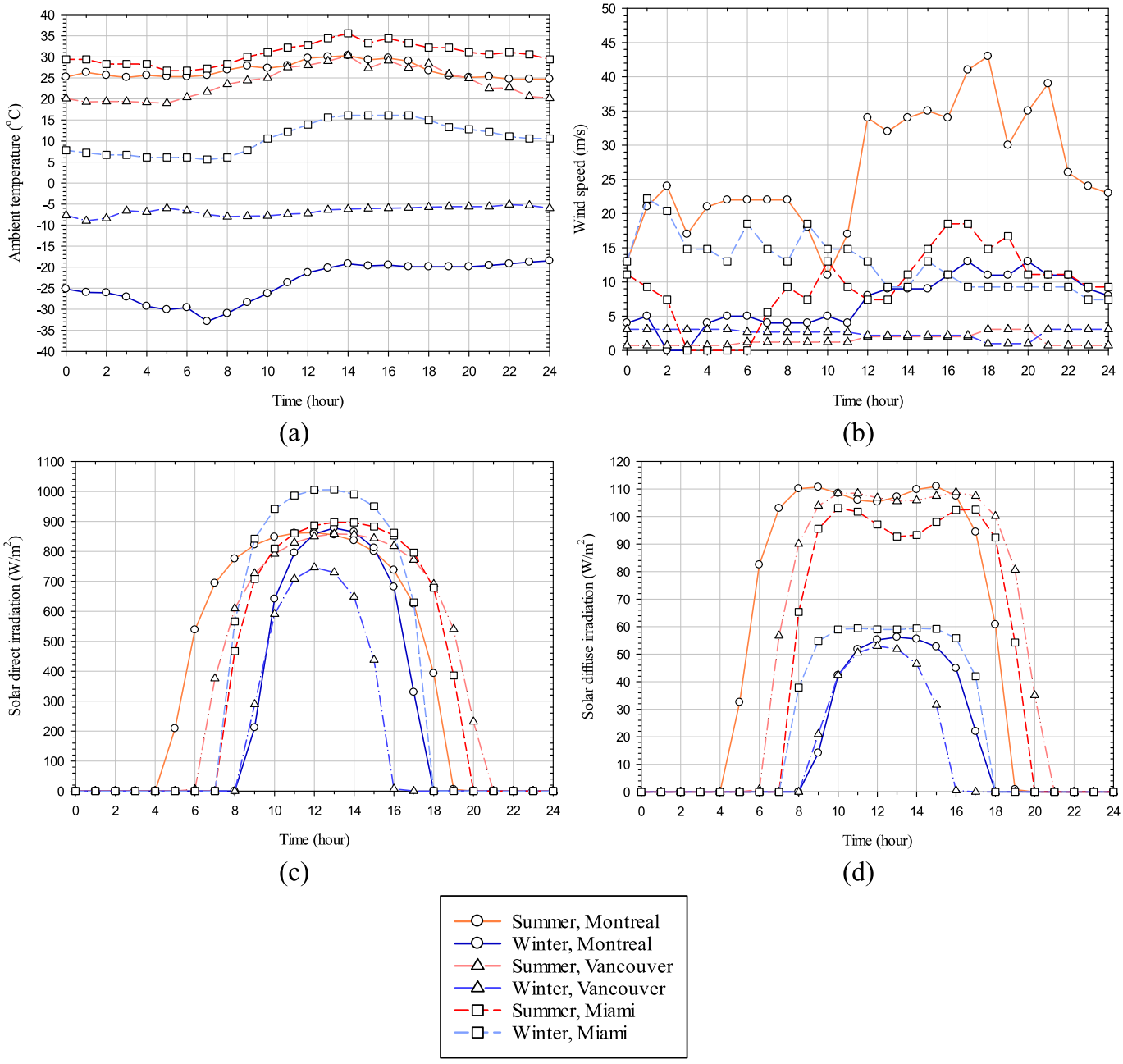

Fig.2. Climate data for Montreal, Vancouver, and Miami in summer and winter: (a) Ambient temperature [26,27], (b) Wind speed [26,27], (c) Solar direct irradiation [22], and (d) Solar diffuse irradiation [22].

$$\beta = \begin{cases} 0 if T \le T_{opaqueus} \\ 1 if T \ge T_{transparentus} \\ \dfrac{T - T_{opaqueus}}{T_{transparentus} - T_{opaqueus}} if T_{opaqueus} < T < T_{transparentus} \end{cases} \quad (12)$$

The term S_h in Eq. (8) denotes the volumetric heat source/sink related to phase change, which is defined as:

$$S_h = -\frac{\partial(\rho \Delta H)}{\partial t} \quad (13)$$

- Radiation equation:

In this study, the Discrete Ordinates (DO) model is adopted to simulate radiation effects because it offers the most comprehensive treatment of radiation in ANSYS FLUENT [22]. This model enables the simulation of radiation scattering and absorption across various optical thicknesses. By converting the radiation heat transfer equation into a transport equation for radiation intensity and solving it across a finite number of discrete solid angles [22], the DO model enhances precision. However, the increased number of equations required by the DO model slows down the simulation process.

The radiative transfer equation for an absorbing, emitting, and scattering medium at position $\vec{r}$ in the direction $\vec{s}$ is [22]:

$$\frac{dI(\vec{r},\vec{s})}{ds} + (\sigma_a + \sigma_s) I(\vec{r},\vec{s}) = an^2 \frac{\sigma T^4}{\pi} + \frac{\sigma_s}{4\pi} \int_0^{4\pi} I(\vec{r},\vec{s}') \varnothing(\vec{s}.\vec{s}') d\Omega' \quad (14)$$

The DO model considers the radiative transfer equation in the direction $\vec{s}$ as a field equation and is written as [22]:

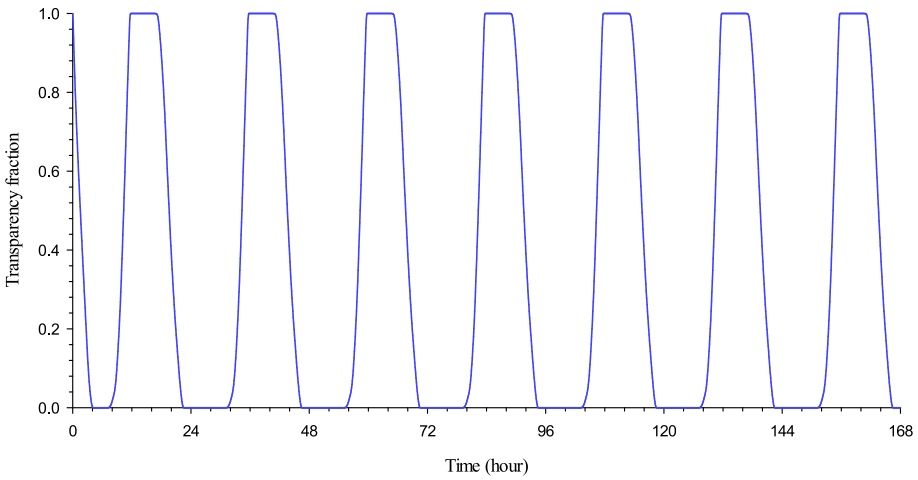

Fig.3. Transparency fraction of the DGW-SSPCM system in 7 days.

$$\nabla.(I(\vec{r},\vec{s})\vec{s})+(\sigma_a+\sigma_s)I(\vec{r},\vec{s})=an^2\frac{\sigma T^4}{\pi}+\frac{\sigma_s}{4\pi}\int_0^{4\pi}I(\vec{r},\vec{s}')\varnothing(\vec{s}.\vec{s}')d\Omega' \quad (15)$$

In Eqs. (14) and (15), I, n, $\vec{r}$, $\vec{s}$, $\vec{s}'$. $\varnothing$, Ω', and σ represent radiation intensity, refractive index, position vector, direction vector, scattering direction vector, phase function, solid angle, and the Stefan-Boltzmann constant (5.67×10^{-8} W/m^{2}K^4), respectively.

2.4. Weather conditions

The glazing system in this study represents a south-facing window located in Montreal, Vancouver, and Miami. For Montreal, the coordinates are 45.52°N latitude and 73.42°W longitude. The coldest and hottest days selected for this study in Montreal are January 22nd and July 21st, 2022. The time zone is GMT-5 during Eastern Standard Time (EST) and GMT-4 during Eastern Daylight Time (EDT). Montreal's climate code based on the Köppen-Geiger classification [25] is Dfb, representing a humid continental climate with warm summers and no dry season. For Vancouver, the coordinates are 49.3°N latitude and 123.12°W longitude. The selected coldest and hottest days in Vancouver are December 22nd and July 29th, 2022. The time zone is GMT-8 during Pacific Standard Time (PST) and GMT-7 during Pacific Daylight Time (PDT). Vancouver's climate code based on the Köppen-Geiger classification [25] is Cfb, representing a temperate oceanic climate with warm summers and no dry season. For Miami, the coordinates are 25.76°N latitude and 80.19°W longitude. The coldest and hottest days chosen for this study in Miami are January 30th and August 18th, 2022. The time zone is GMT-5 during Eastern Standard Time (EST) and GMT-4 during Eastern Daylight Time (EDT). Miami's climate code based on the Köppen-Geiger classification [25] is Aw, representing a tropical savanna climate with a distinct dry season in winter. All climatic conditions are considered for both sunny and cloudy days on the hottest and coldest days of the year. The ambient weather conditions include hourly wind speed [26,27], hourly ambient temperature [26,27], hourly solar direct irradiation [22], and hourly solar diffuse irradiation [22], for the coldest and hottest days, as depicted in Fig. 2.

2.5. Initial and boundary conditions

The initial temperatures for all components of both the DGW-REF and DGW-SSPCM configurations are set to 26 °C for summer and 24 °C for winter. The side surfaces (exterior top, bottom, front, and back) of the window are treated as thermally insulated or adiabatic (i.e., no energy transport on these sides). The interface between two material layers is modeled using coupled thermal boundary conditions and semi-transparent radiation boundary conditions, ensuring continuity of temperature and heat flux across the real and shadow surfaces while allowing incoming radiation to pass through the surface. In this study, all material layers are assumed to be in perfect thermal contact. This means that the thermal contact resistances at the interfaces of material layers are set to zero. Mixed thermal boundary conditions, which include both convection and radiation, are applied to the window's indoor and outdoor surfaces.

Therefore, it is necessary to determine parameters such as the heat transfer coefficient, free stream temperature, external emissivity, and external radiation temperature for these surfaces. Furthermore, to account for solar irradiation within the numerical domain, semi-transparent boundary conditions are established. This necessitates defining parameters like direct solar irradiation, diffuse solar irradiation, and the beam direction vectors in the x, y, and z directions for both indoor and outdoor surfaces. The emissivity of typical clear glass is set at 0.9 [28] for all boundaries. The sunshine factor is set to 1 to represent a sunny day and to 0 for a cloudy day, which results in zero direct solar irradiation.

For the window's indoor surface thermal and radiation boundary conditions, the heat transfer coefficient is set to 8.7 W/m2K [29]. The free stream temperature and external radiation temperature are both set to 26 °C in summer and 24 °C in winter. No solar irradiation is applied to the indoor radiation boundary condition to obviously not model a direct or diffuse solar irradiation to the indoor surface. In summary, the boundary condition on the outdoor surface is heat flux with $q_{h,outd}$. Also, the boundary condition on the indoor surface is heat flux with $q_{h,ind}$. Both $q_{h,outd}$ and $q_{h,ind}$ account for heat transfer by convection, radiative heat exchange between these surfaces and the the environment (sky conditions, ground, adjacent constructions/buildings, wind speed, cloud index, etc.). The detailed procedure for determining both $q_{h,outd}$ and $q_{h,ind}$ are available in [30]. In this procedure, the hourly cloud index is 1.0 for overcast conditions and 0 for clear conditions.

For the window's outdoor surface thermal and radiation boundary conditions, all parameters except emissivity are imported into ANSYS FLUENT using User Defined Functions (UDFs) written in C programming, compatible with the FLUENT library, to simulate a full 24-hour day. These UDFs utilize piecewise linear functions to incorporate the hourly weather data. The hourly ambient temperature is used for the free stream temperature in the thermal boundary condition. Additionally, hourly values for direct and diffuse solar irradiations, as well as the x, y, and z beam direction vectors, are set in the radiation boundary conditions. The hourly heat transfer coefficient, which depends on wind speed, and the hourly external radiation temperature or sky temperature, which depends on ambient temperature, are calculated using Eqs. (16) and (17) [31].

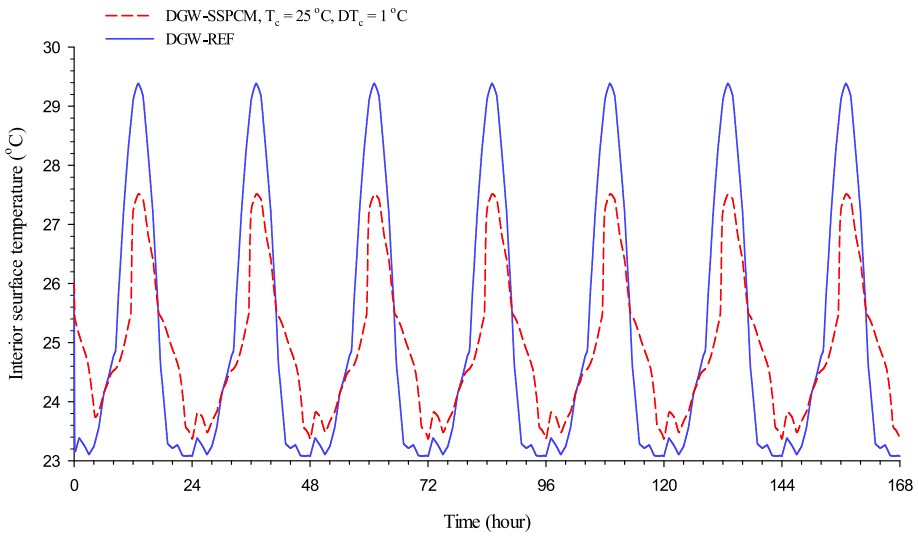

Fig.4. Interior surface temperature of the systems DGW-REF and DGW-SSPCM in 7 days.

Table 3
Thermal energy values for single summer design day duplicated 7 times.

Thermal energy (kJ)	DGW-REF	Deviation (%)	DGW-SSPCM	Deviation (%)
Day 1 (Round 1)	99.6971	–	89.1331	–
Day 2 (Round 2)	99.4057	0.29	86.2118	3.28
Day 3 (Round 3)	99.4057	0	86.2118	0
Day 4 (Round 4)	99.4057	0	86.2118	0
Day 5 (Round 5)	99.4057	0	86.2118	0
Day 6 (Round 6)	99.4057	0	86.2118	0
Day 7 (Round 7)	99.4057	0	86.2118	0

$$h_a = 5.62 + 3.9v_{wind} \tag{16}$$

$$T_{sky} = 0.0552T_{air,o}^{1.5} \tag{17}$$

In Eq. (16), h_a in W/m^{2}K and v_{wind} in m/s. Also, both T_{sky} and $T_{air,o}$ in Eq. (17) are in K.

2.5.1. Study of initial condition effects

As previously mentioned, the initial conditions were assumed for this analysis. In this section, we examine the impact of these assumed initial conditions on the results. To investigate the effect of the assumed initial conditions on thermal performance, numerical simulations were conducted over a period of 7 consecutive days. The thermal performance of the glazing system at a specific location is influenced by hourly weather data. By utilizing the hourly weather data for the simulation period (i.e., 7 days), the variations in thermal performance over time are contingent upon two primary factors: (a) the assumed values of the initial conditions and (b) the temporal fluctuations in the weather data. To isolate the influence of factor (b), the weather data from Day 1, where the assumed initial conditions were applied, was replicated for the subsequent days. Consequently, any observed changes in thermal performance over time can be attributed predominantly to the assumed initial conditions. The case under study is for DGW-SSPCM in Montreal with phase transition temperature (T_c) of 25 °C and phase transition temperature range (ΔT_c) of 1 °C, in which the SSPCM experiences a full phase transition. Fig. 3 presents the transparency fraction of the DGW-SSPCM system over 7 simulated days. The repeated cycle shows how the transparency fraction stabilizes after the first day, demonstrating that the assumed initial condition effects are effectively eliminated. Fig. 4 illustrates the interior surface temperature of both the DGW-REF and DGW-SSPCM systems over the same 7-day period. A comparison of

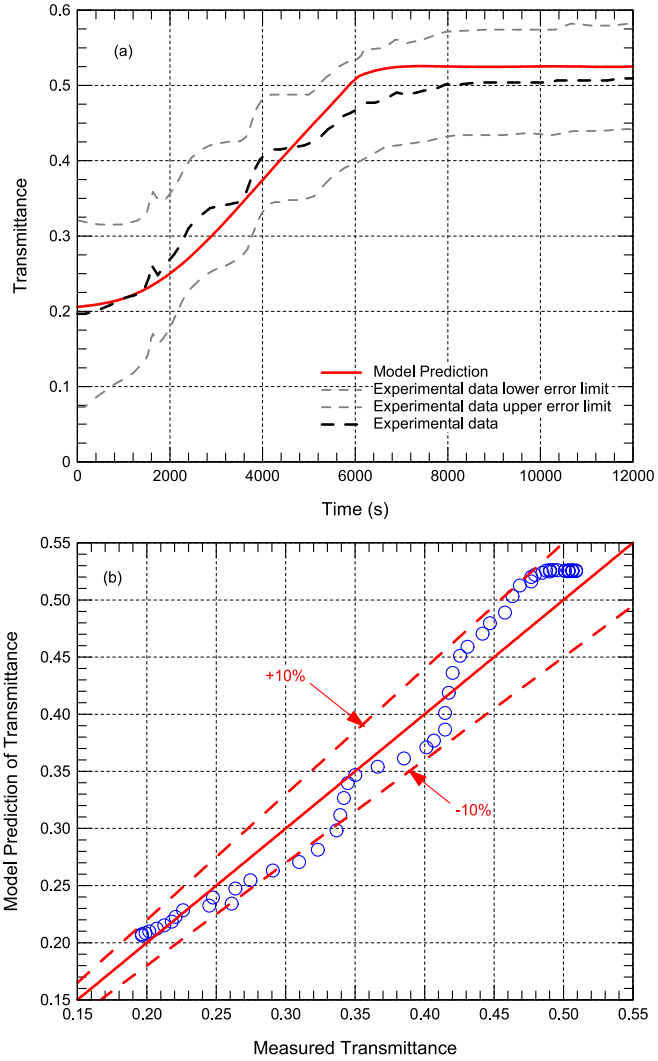

Fig.5. Current numerical model results compared to the experimental data [20].

Table 4
Grid sensitivity analysis.

Case	Number of elements	$\overline{q''}$(W/m^2)	Error (%)
1	288,923	15.47104	
2	158,661	15.5293	0.376595
3	82,369	15.58556	0.740245
4	27,440	15.71381	1.569181
5	11,025	15.8746	2.608495
6	4050	16.1296	4.25671

the curves shows that, after the first day, the temperature variations become stable (i.e., the assumed initial conditions have no effect). Table 3 provides the deviation percentage for both systems over the 7 simulated days, which is defined as: ((Thermal energy of current round − Thermal energy of previous round) / Thermal energy of previous round) × 100 %. The DGW-REF system exhibits a minor deviation of 0.29 % on Day 2, which becomes negligible for the remaining days, indicating consistency after the second day. For the DGW-SSPCM system, although the deviation on Day 2 is 3.28 %, this value is sufficiently low to be considered negligible for the simulations, in order to reach a precise solution with the minimum computational cost. The system achieves 0 % deviation from Day 3 onward.

3. Numerical procedure

3.1. Model description

The commercial CFD code ANSYS FLUENT (version 2022 R1) is used, employing the SIMPLE algorithm for velocity–pressure coupling. Design Modeler and Ansys Meshing were utilized to generate the geometry and grid, respectively. For the discretization of pressure, momentum, and energy, a second-order upwind scheme is applied, while the DO model and transient formulation use a first-order upwind and first-order implicit scheme, respectively. The convergence criteria were set to be less than 10^{-6}, 10^{-6}, 10^{-6}, 10^{-6}, 10^{-9}, and 10^{-9} for mass conservation, x-velocity, y-velocity, z-velocity, energy and DO-intensity, respectively.

3.2. Model validation

In this research, the model traditionally used for SLPCMs has been adapted for SSPCMs through the solidification/melting model. The key difference is that SSPCMs do not exhibit natural convection because they do not have a liquid phase when melting. By disregarding the gravity effect and accounting for the high viscosity of the SLPCM's liquid phase, its behavior can be approximated to that of an SSPCM.

To validate the numerical model that includes the Discrete Ordinates (DO) model and the solidification/melting model in glazing systems, transient numerical results over a simulation period of 12,000 s were compared with experimental data from Gowreesunkera et al. [20] concerning the transmittance of PCM-filled glazing units over time. In their study, the researchers developed an experimental setup to measure the changes in radiation effects within the mushy phase, which is not possible with a spectrophotometer alone. This setup provided a realistic depiction of the radiation behavior in a PCM-glazed system. The entire setup was placed in an environmental chamber with controlled air temperature. A 150 W metal halide lamp emitting diffuse neutral white light was used as the light source. The regular double glazing measured 20 cm by 20 cm with a total thickness of 24 mm, consisting of 4 mm glass, a 16 mm air cavity, and another 4 mm glass layer. In the PCM-filled glazing configuration, the air cavity was replaced with RT27. The irradiation level and initial PCM/air temperature were set to 950 W/m^2 and 13 °C, respectively.

In this study, the experimental data by Gowreesunker et al. [20] was used to validate the present model. This data is provided in Fig. 5a by the black-dashed curve. Due to the uncertainties in the measurements, the upper and lower error limits are also provided in this figure by dashed-gray curves. In this figure, the overall transmittance was defined by the ratio of radiation flux between the front and back faces. As shown in Fig. 5a, the transmittance values from the simulation, shown by the red curve, are in close agreement with the experimental data, with variations staying within the margin of error. Additionally, the observed transmittance trends exhibit similarity between the simulation results and the experimental data. However, in this figure, it is visible that in some areas the simulation results and experimental data do not match well. It can be attributed to the enthalpy-porosity model, which assumes a linear relationship between temperature and the liquid fraction within the phase change temperature range. This model treats the mushy zone as a porous medium, with the porosity linearly dependent on the local

Table 5
Time-step sensitivity analysis.

Case	Time step size	$\overline{q''}$(W/m^2)	Error (%)
1	10 sec	15.73079	
2	30 sec	15.72085	0.06315
3	1 min	15.70591	0.15812
4	2.5 min	15.66088	0.44443
5	5 min	15.58556	0.92319
6	10 min	15.43214	1.89849
7	20 min	15.11929	3.88729
8	30 min	14.82675	5.74694

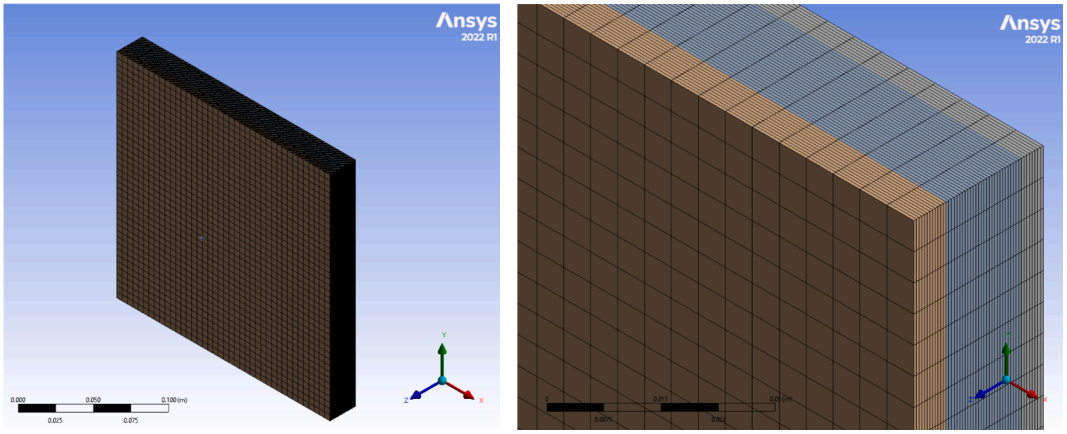

(a) (b)

Fig.6. The generated grid in this study: (a) the entire domain and (b) a zoomed-in view.

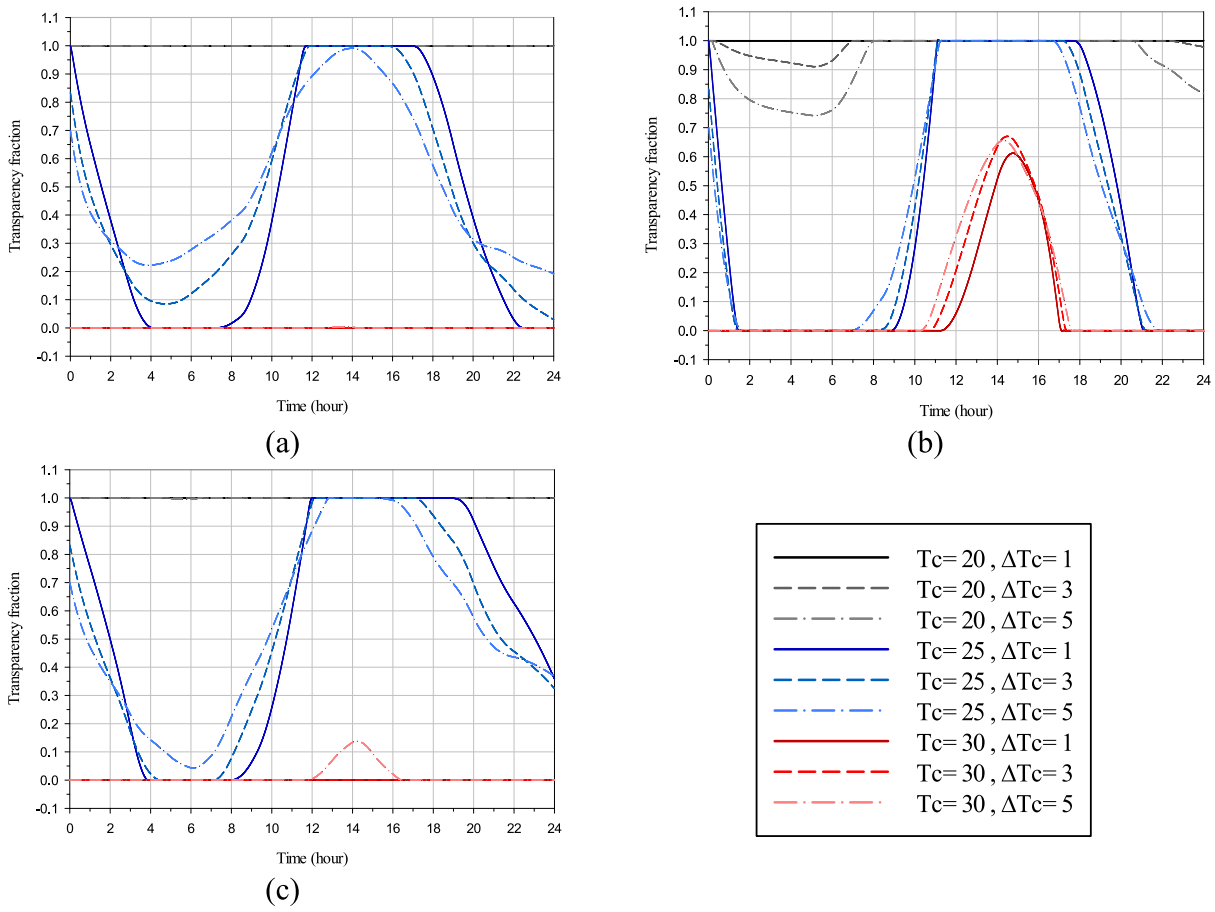

Fig.7. SSPCM's transparency fraction variations in summer sunny conditions for (a) Montreal, (b)Vancouver, (c) and Miami.

temperature. This assumption simplifies the modeling of melting and solidification, creating discrepancies between numerical results and experimental data, especially when a non-linear jump is observed in the experimental results. As the numerical results are in agreement with the experimental data being within ± 10 % as shown in Fig. 5b, the numerical model is validated and can be reliably used in this study.

3.3. Grid sensitivity

To determine the optimal grid size for a mesh-independent solution, various grid sizes, from fine to coarse, were generated over the numerical domain of a DGW-SSPCM. The mean total heat flux over a 24-hour period, as described in Eq. (18), on the interior surface of the inner glass pane was used as the criterion for assessing grid independence. The results are presented in Table 4. According to this table, a grid size with 82,369 elements was found to be approximately optimal, as its relative error is less than 1 %. Therefore, this grid size was used in the study. For the grid size with 82,369 elements used in this study, the grid generated in the computational domain is displayed in Fig. 6, including both an overview of the entire domain and a zoomed-in view.

$$\overline{q''} = \frac{1}{t}\int_0^t q'' dt \tag{18}$$

3.4. Time step sensitivity

The aim of the time step sensitivity analysis is to identify the largest time step size that maintains accuracy. Following the same method as in the previous section, the average total heat flux over a 24-hour period on the interior surface of the inner glass pane was used to determine the optimal time step size, aiming to minimize CPU time. Table 5 presents the results for various time step sizes. It indicates that a time step size of 5 min results in a relative error of less than 1 % and is appropriate for use in the simulations.

4. Results and discussion

Numerical simulations are performed for the scenarios outlined in Table 2. These simulations span a 24-hour real-time period, covering both sunny and cloudy days during the coldest and hottest days of 2022 in Montreal, Vancouver, and Miami. The parametric study is conducted to analyze the effects of various parameters, including phase transition temperature (T_c) and phase transition temperature range (ΔT_c), as well as four climatic conditions (summer sunny, summer cloudy, winter sunny, and winter cloudy), on transparency fraction, interior surface temperature, total heat flux on the interior surface, and the glazing system's energy savings.

4.1. Transparency fraction

This section analyzes the variations in the transparency fraction of the SSPCM, defined in Eq. (12), for the scenarios outlined in Table 2 during summer and winter, focusing on the hottest and coldest sunny and cloudy days.

Fig. 7 illustrates the variations of the transparency fraction of the SSPCM in summer sunny days in the three studied cities for all cases. According to this figure, the transparency fraction displays distinct diurnal patterns across all locations, influenced by phase transition temperature (T_c) and phase transition temperature range (ΔT_c). The transparency fraction increases from 0 to 1 as the temperature rises,

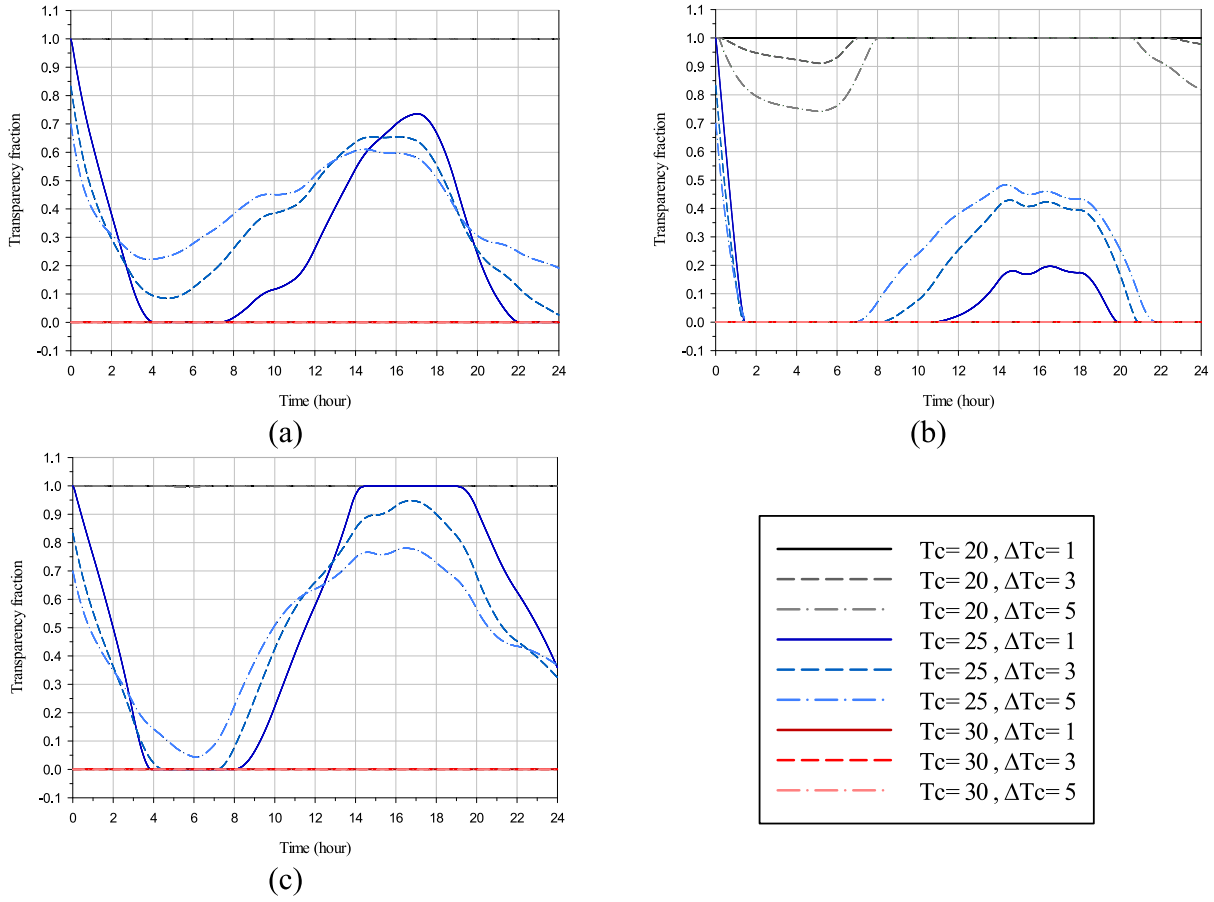

Fig.8. SSPCM's transparency fraction variations in summer cloudy conditions for (a) Montreal, (b)Vancouver, (c) and Miami.

indicating the SSPCM is storing heat using its high latent heat thermal energy storage. Conversely, it decreases from 1 to 0 as the temperature falls, releasing stored heat to the surroundings. In Montreal, Fig. 7a, the transparency fraction increases sharply in the morning, peaking around noon, and decreases towards the evening. Notably, at T_c = 20 °C, the transparency fraction remains at 1 throughout the day, providing continuous visual clarity. Conversely, at T_c = 30 °C, the transparency fraction stays at 0, indicating the SSPCM remains opaque. At T_c = 25 °C the SSPCM has undergone a full phase transition in which smaller ΔT_c values result in sharper transitions, while larger ΔT_c values delay this transition. However, it is important to note that when the SSPCM does not experience a full phase transition, the glazing system cannot benefit from its high latent thermal storage capability. Vancouver, Fig. 7b, exhibits a different pattern. At T_c = 20 °C, although the SSPCM remains transparent throughout the day, it reaches the translucent phase at night for ΔT_c = 3°C and ΔT_c = 5°C. Similarly, at T_c = 30 °C, the SSPCM also undergoes partial phase transitions, becoming translucent during the warmest part of the day and returning to an opaque state in the evening. This partial phase transition behavior limits the full utilization of the SSPCM's latent heat storage capability. In the meanwhile, the full phase transition is achieved at T_c = 25 °C, being transparent during the office hours. The transparency fraction in Miami, Fig. 7c, is similar to Montreal. The SSPCM stays transparent and opaque throughout the day at T_c = 20 °C and T_c = 30 °C, respectively, and goes a full transition at T_c = 25 °C by staying transparent during the office hours. However, the SSPCM experiences more prolonged periods of partial transparency, likely due to higher ambient temperatures. Larger ΔT_c values (e.g., 5 °C) result in more gradual changes in transparency, while smaller ΔT_c values (e.g., 1 °C) cause sharper transitions. This is evident across all locations, with ΔT_c = 1°C curves showing the steepest transitions. Overall, Montreal and Vancouver exhibit similar trends with slight variations in transition timings and transparency duration, attributed to climatic differences. Three cities benefit from SSPCM's transparency aligning with office hours, enhancing the utility of SSPCM in commercial buildings. Miami's higher average temperatures lead to more sustained periods of partial transparency, reflecting the SSPCM's behavior under consistently warmer conditions. This partial transparency is less critical for visual clarity during office hours but may still provide adequate daylighting for residential buildings.

Fig. 8 explores the behavior of the SSPCM's transparency fraction in summer cloudy conditions for Montreal, Vancouver, and Miami. In Montreal and Vancouver, Fig. 8a and 8b, the full phase transition of the SSPCM does not occur for all scenarios due to the lack of direct solar irradiation, while it occurs in Miami according to higher ambient temperatures. In three cities, only at T_c = 25 °C partial phase transition of the SSPCM occurs, indicating the impact of cloud cover on the SSPCM's performance. The SSPCM's performance in cloudy conditions is characterized by less distinct and lower peaks in transparency fraction compared to sunny conditions, as seen in Fig. 7. The reduced solar heating on cloudy days limits the SSPCM's ability to fully transition, thereby impacting its heat storage and release capabilities. Higher ΔT_c values result in more extensive phase transitions of the SSPCM, but these transitions occur more abruptly compared to those with lower ΔT_c values. The intermediate T_c value of 25 °C provides a better balance, ensuring some level of transparency during office hours, enhancing both visual comfort and energy efficiency.

Fig. 9 illustrates the variations of the transparency fraction of the SSPCM in winter sunny conditions for the three studied cities. In Montreal, Fig. 9a, the transparency fraction shows significant changes throughout the day. At T_c = 10 °C, the transparency fraction drops

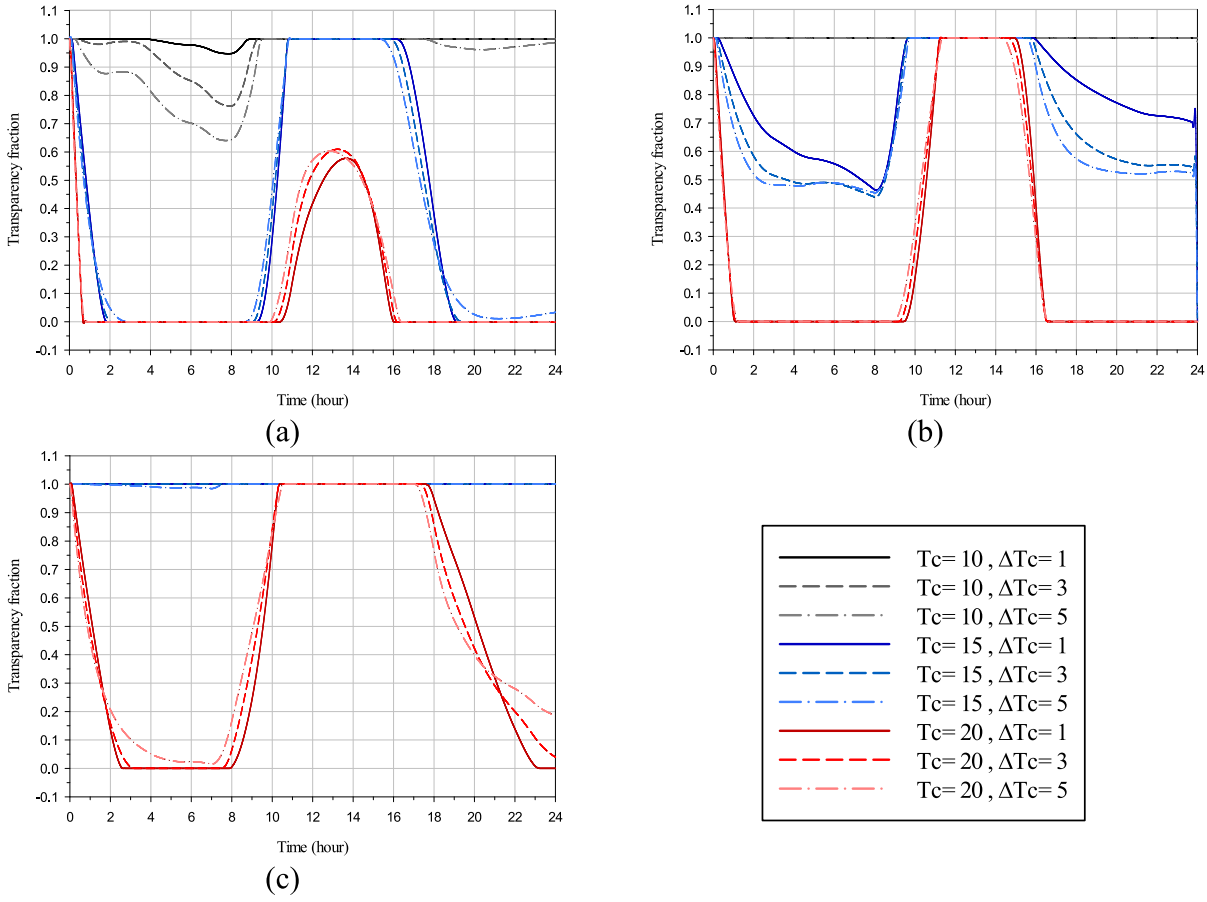

Fig.9. SSPCM's transparency fraction variations in winter sunny conditions for (a) Montreal, (b)Vancouver, (c) and Miami.

during the night partially (more reduction in higher ΔT_c) and SSPCM falls into translucent phase and by the appearance of the sun it returns back to the opaque phase. At $T_c = 20$ °C, a partial phase transition from transparent to translucent is visible and SSPCM doesn't go under a full phase transition. For $T_c = 20$ °C, the full phase transition is visible and ΔT_c has little impact on the transparency fraction. The SSPCM stays transparent during the office hours and opaque in the rest of the day, making it suitable for commercial buildings. In Vancouver, Fig. 9b, the transparency fraction also varies throughout the day but with distinct patterns for different T_c values. At $T_c = 10$ °C, the transparency fraction remains close to 1 for most of the day, indicating consistent transparency. Due to warmer winters in Vancouver compared to Montreal, the SSPCM stays translucent and transparent for $T_c = 20$ °C and $T_c = 15$ °C, during the night and stays transparent during the day. This indicates that Vancouver's climate may allow for a more stable transparency fraction with intermediate T_c values, balancing visual clarity and thermal storage. Due to even warmer winters in Miami, Fig. 9c, the transparency fraction demonstrates highest values throughout the day for $T_c = 10$ °C and $T_c = 15$ °C, maintaining constant transparency. For $T_c = 20$ °C, the full phase transitioning of the SSPCM provides the high latent thermal storage to the glazing system by staying opaque at night and transparent during the night, making it effective for maintaining visual clarity while utilizing the SSPCM's thermal storage capabilities. Overall, in winter sunny conditions, the SSPCM shows effective heat storage and release patterns across all three cities, with notable transparency peaks during midday. Proposing a system that offers a balanced approach, ensuring transparency during key daylight hours while leveraging the SSPCM's thermal storage potential differs from city to city as $T_c = 15$ °C yields such a system in Montreal, but it is $T_c = 20$ °C in Vancouver and Miami. This behavior highlights the importance of selecting appropriate T_c values based on specific climatic conditions to optimize the performance of SSPCMs in double glazing systems.

Fig. 10 depicts the changes in the transparency fraction of the SSPCM under winter cloudy conditions for the three examined cities. the SSPCM's performance in winter cloudy conditions is characterized by lower and less distinct peaks in transparency fraction compared to sunny conditions, as seen in Figs. 7 and 9. The reduced solar heating due to the absence of direct solar irradiation on cloudy days limits the full phase change transition of SSPCM, thereby impacting its heat storage and release capabilities. In Montreal, Fig. 10a, The SSPCM experiences small phase transitions, particularly at $T_c = 10$ °C and higher ΔT_c values. In Vancouver, Fig. 10b, at $T_c = 15$ °C, the SSPCM stays in the translucent phase all day long, with lower ΔT_c values showing higher transparency fraction fluctuations. In Miami, Fig. 10c, the transparency fraction demonstrates a pattern of partial transparency with peaks occurring later in the day. At $T_c = 20$ °C, the transparency fraction shows partial phase transitions, which are stronger with higher ΔT_c values, but remains mostly opaque throughout the day. The comparison between sunny and cloudy conditions underscores the need to consider weather variability in the application of SSPCMs for energy efficiency and visual comfort.

4.2. *Interior surface temperature*

This section discusses the simulation results pertaining to the variations in the interior surface temperature of the glazing system during the hottest summer and coldest winter days under both sunny and cloudy sky conditions.

Fig. 11 illustrates the variations of the interior surface temperature of the double-glazed window equipped with SSPCM in summer sunny

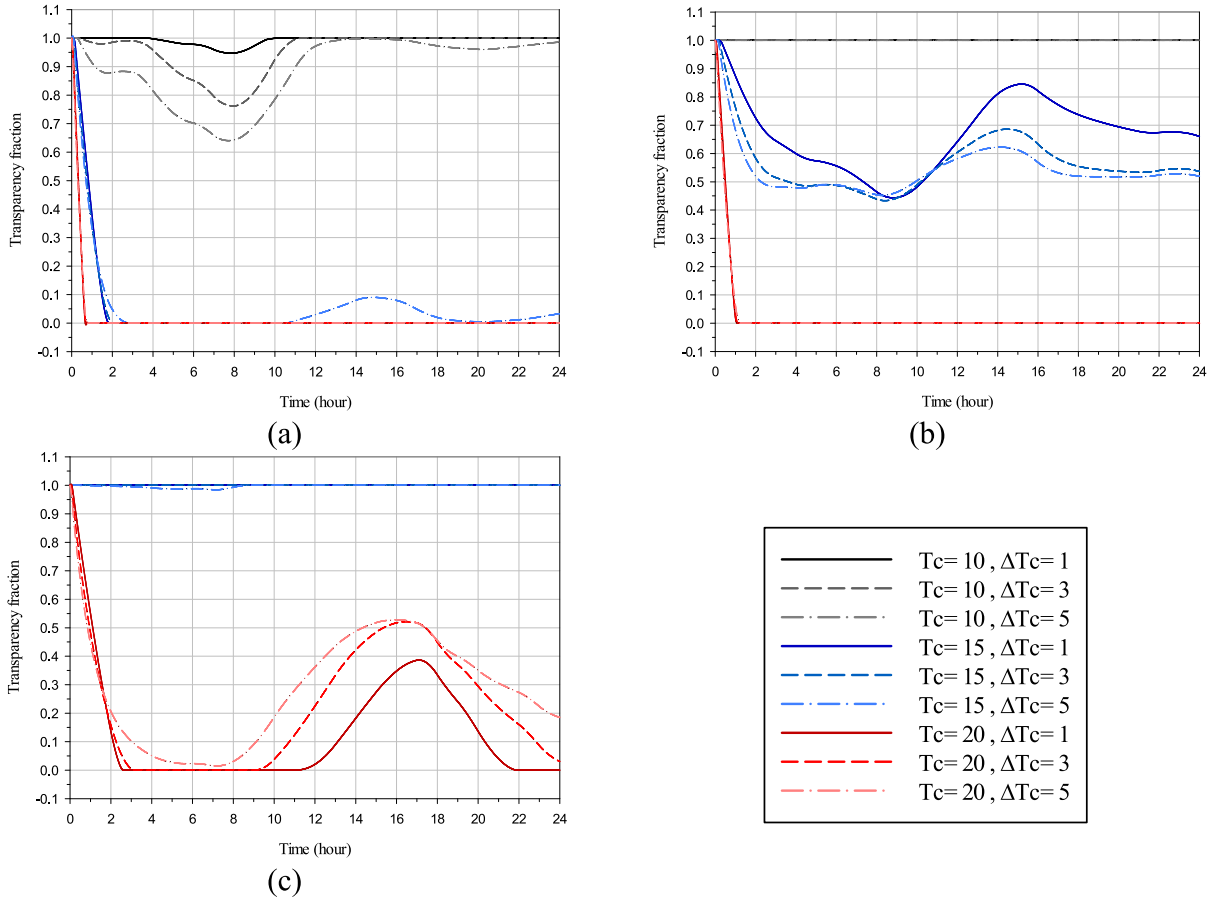

Fig.10. SSPCM's transparency fraction variations in winter cloudy conditions for (a) Montreal, (b) Vancouver, (c) and Miami.

conditions for the three studied cities. The interior surface temperature is crucial for maintaining thermal comfort, with lower temperatures preferred in summer. In Montreal, Fig. 11a, the use of SSPCM at T_c = 25 °C and ΔT_c = 5°C has reduced the interior surface temperature by nearly 2 °C at the peak cooling load demand. This reduction is achieved by utilizing the SSPCM's capability to store direct solar irradiation, preventing it from entering the building. According to Fig. 11a, only at T_c = 25 °C does the SSPCM undergo phase transition, which results in a different temperature trend in Fig. 11a compared to the other two T_c values. At T_c = 25 °C, lower temperatures are achieved, thus providing better thermal comfort. During the day, the SSPCM absorbs solar heat, utilizing its high latent heat thermal storage capability, which is evident as the interior surface temperature is lower (leading to energy savings during peak load hours). At night, the stored heat is released, resulting in higher interior surface temperatures. Additionally, lower ΔT_c values cause lower interior surface temperatures with sharper gradients. In Vancouver, the use of SSPCM has also reduced the interior surface temperature by around 0.8 °C at T_c = 30 °C and ΔT_c = 1°C at the peak cooling load demand, which is less than the reduction observed in Montreal. This is due to the faster phase transition of the SSPCM caused by higher ambient temperatures. The interior surface temperature reduction in Miami is almost similar to Vancouver, due to the rapid phase transition of the SSPCM due to higher ambient temperatures. Consequently, the current setup of DGW-SSPCM is more beneficial for thermal comfort under Montreal's summer sunny climatic conditions. In addition, the importance of selecting appropriate T_c and ΔT_c values based on specific climatic conditions to optimize the performance of SSPCMs in double glazing systems for improved thermal comfort in summer is evident.

Fig. 12 displays the variations of the interior surface temperature of the studied scenarios in summer cloudy conditions for the three studied cities. In Montreal, Fig. 12a, the SSPCM with T_c = 25 °C and ΔT_c = 1°C shows nearly a 1 °C reduction in the interior surface temperature during the peak load hour. The SSPCM stores heat during the day, providing thermal comfort during peak hours, and releases it at the start of the evening, thereby smoothing temperature fluctuations. Similarly, in Vancouver, Fig. 12b, the SSPCM with T_c = 25 °C and ΔT_c = 1°C also reduces the interior surface temperature, though the reduction is less pronounced than in Montreal. The SSPCM effectively stores heat during the day and releases it in the evening, helping to smooth out temperature variations and improve thermal comfort. In Miami, Fig. 12c, the SSPCM with T_c = 25 °C and ΔT_c = 1°C significantly reduces the interior surface temperature and smooths out fluctuations. The impact is more pronounced due to the warmer climate, with the SSPCM storing more heat during the day and releasing it in the evening, maintaining lower interior surface temperatures and enhancing thermal comfort during peak load hours. Similar to summer sunny climatic conditions, in summer cloudy conditions, the DGW-SSPCM has been more advantageous in Montreal for improving thermal comfort compared to the other two cities. The ability of the SSPCM to effectively store and release heat, thereby moderating the interior surface temperature, underscores its potential for enhancing thermal comfort and reducing cooling loads in buildings.

Fig. 13 displays the variations of the interior surface temperature of the DGW-SSPCM in winter sunny conditions for the three studied cities. The interior surface temperature is crucial for maintaining thermal comfort, with higher temperatures preferred in winter. In Montreal Fig. 13a, the SSPCM blocks a significant amount of solar heat during the day, creating a noticeable difference between the interior surface temperatures of DGW-SSPCM and DGW-REF. At T_c = 15 °C, the stored heat

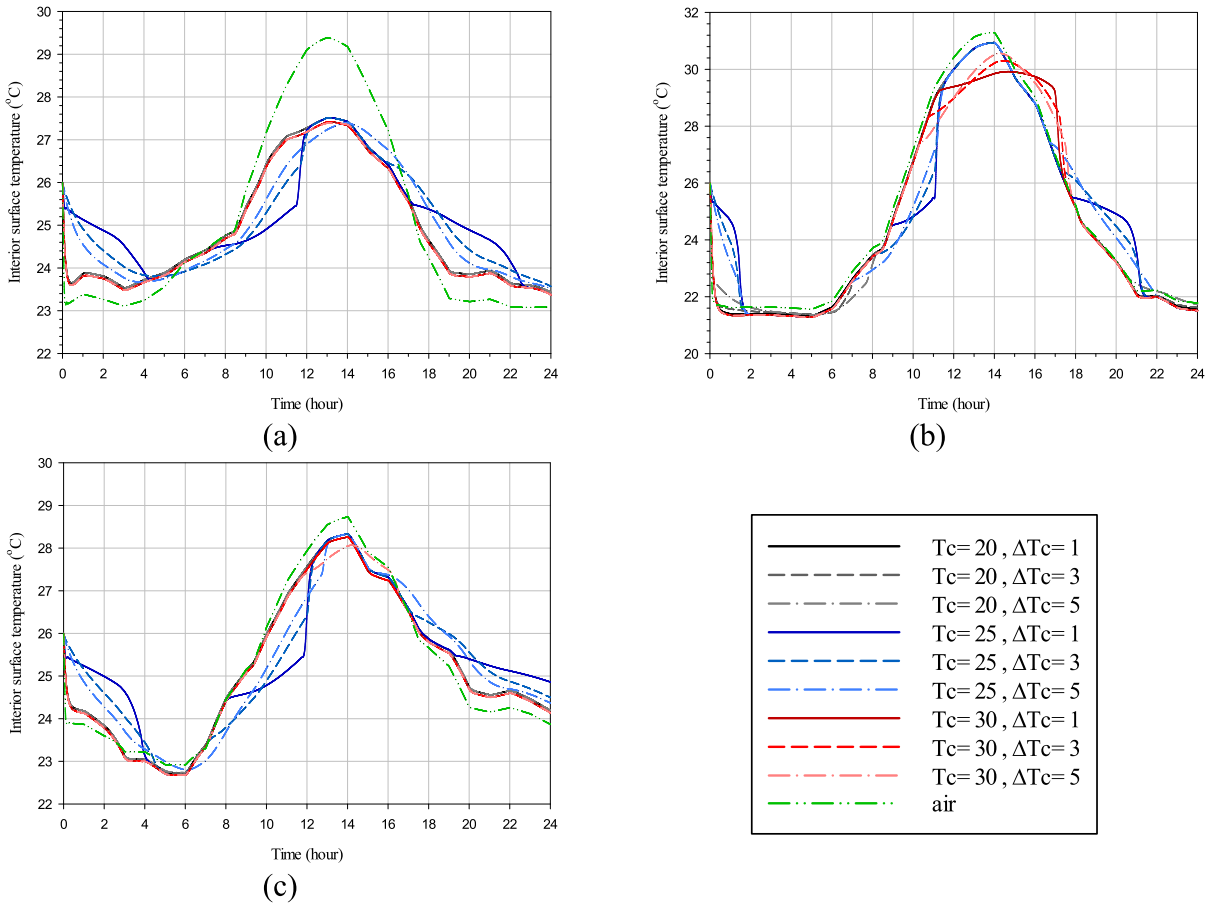

Fig.11. SSPCM's interior surface temperature variations in summer sunny conditions for (a) Montreal, (b)Vancouver, (c) and Miami.

is released to the interior at the start of the evening, enhancing the interior surface temperature and improving thermal comfort during these hours when heating demand is higher, as the SSPCM undergoes a full phase transition at this temperature. In Vancouver Fig. 13b, a similar pattern occurs for the interior surface temperature, but with a smaller temperature reduction for DGW-SSPCM compared to DGW-REF during the day and a noticeable temperature increase at the start of the evening at $T_c = 20$ °C. In Miami, Fig. 13c, the released heat is more significant, causing the interior surface temperature to increase from the start of the evening until midnight due to the warmer winters in Miami.

Fig. 14 shows the interior surface temperature distribution for the studied cases in winter cloudy conditions for the three cities. In Montreal and Vancouver, Fig. 14a and 14b, due to the lack of direct solar irradiation, the presence of SSPCM appears to worsen the interior surface temperature. This is because of the system's lower thermal resistance and the absence of thermal inertia utilization, which prevents effective heat retention and release. Without sufficient solar energy, the SSPCM cannot undergo a full phase change cycle, thereby diminishing its ability to regulate the interior temperature effectively. However, in Miami Fig. 14c, the situation is different. There has been enough ambient heat to cause the SSPCM to store heat during the day through a full phase change cycle. As the ambient temperature drops, the SSPCM releases the stored heat to the surroundings at the start of the evening and continues until midnight. This results in a higher interior surface temperature, contributing to improved thermal comfort during the cooler evening and night hours. The warmer winters in Miami provide a more conducive environment for the SSPCM to function optimally, highlighting the importance of ambient conditions for the effective performance of SSPCM in enhancing thermal comfort.

4.3. Energy performance

To quantify the energy savings or losses of the DGW-SSPCM system compared to the DGW-REF case, we use Eq. (20), which builds on Eq. (19) where thermal energy is defined. In Eq. (19), $\overline{q''}$ represents the mean total heat flux on the interior surface of the inner pane of the DGW, as defined in Eq. (18). This parameter can be either positive or negative, depending on the direction of the heat flux: positive for heat flux from inside to outside and negative for the opposite direction. Energy savings are achieved when the absolute negative value is lower (indicating less total heat flux entering the building) and when the positive value is lower (indicating less total heat flux escaping from the building).

$$E = \overline{q''} \times t \times A \tag{19}$$

$$\Delta E = E_{final} - E_{ref} \tag{20}$$

This section analyzes the thermal energy performance of the proposed glazing system under various sky conditions in three cities: Montreal, Vancouver, and Miami. Table 6 summarizes all the thermal energy values in all the cases outlined in Table 2.

Fig. 15 displays the thermal energy in all studied scenarios, under summer sunny conditions in Montreal, Vancouver, and Miami. In addition, the thermal energy for all studied scenarios is listed in Table 6 for the three analyzed cities under sunny summer climatic conditions. In Montreal, the DGW-SSPCM system achieved energy savings in all cases compared to the DGW-REF system, primarily due to the significant solar energy blockage by the SSPCM, which utilizes its latent thermal storage capacity. As mentioned earlier, negative values represent the total thermal energy entering the building, hence the smaller the absolute value, the greater the energy savings. The energy savings for cases 1 to 9

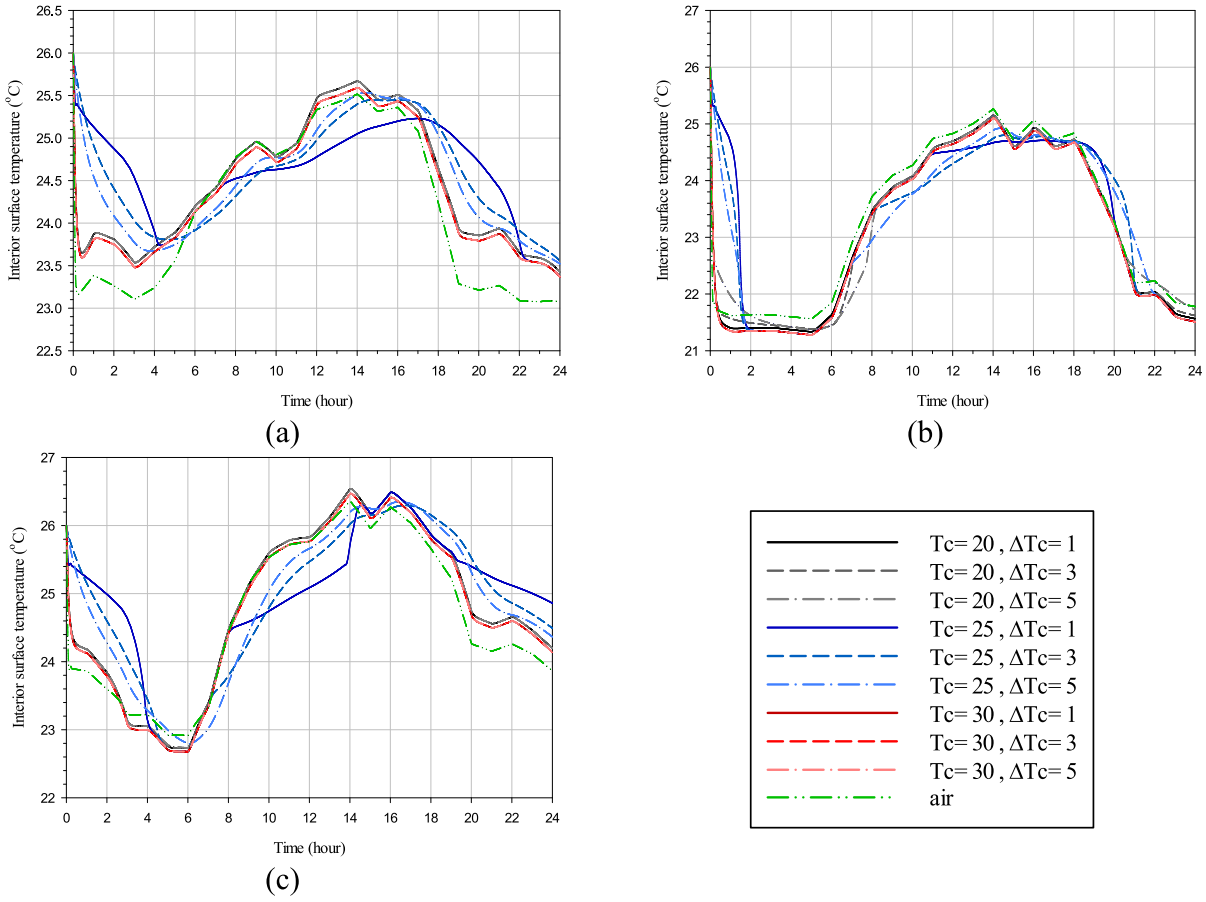

Fig.12. SSPCM's interior surface temperature variations in summer cloudy conditions for (a) Montreal, (b)Vancouver, (c) and Miami.

compared to DGW-REF system are 10.4, 10.4, 10.4, 6.0, 7.2, 9.5, 17.4, 17.4, and 17.4 kJ, respectively. The highest energy savings are observed in the cases 7, 8, and 9 ($T_c = 30\ ^\circ C$), due to the SSPCM remaining opaque throughout the entire day. However, considering the poor visual view of the glazing system in these cases, they are not suitable for fenestration systems. Considering both energy savings and visual clarity, cases 1 to 3 ($T_c = 20\ ^\circ C$) are optimal, as the SSPCM remains in the transparent phase throughout the entire day, providing both energy efficiency and a clear visual view. In cases 4, 5, and 6, the SSPCM undergoes a full phase transition. The lower energy savings of these cases compared to cases 1, 2, and 3, which remained transparent throughout the entire day, can be attributed to the latent thermal heat being released into the indoor environment at night by the SSPCM, due to the latent heat storage during the day. In Vancouver, a similar trend in the behavior of the SSPCM-DGW is observed across scenarios 1 to 9. All cases show energy savings for the DGW-SSPCM system compared to the DGW-REF system, with cases 7, 8, and 9 demonstrating the highest energy savings. The energy savings for cases 1 to 9 compared to DGW-REF system are 17.4, 17.2, 15.8, 9.7, 10.9, 11.9, 21.2, 20.7 and 20.5 kJ, respectively. Comparing the energy savings in the two cities, the energy performance of the SSPCM-DGW system is more beneficial in Vancouver. In Miami, the trend is completely different from the other two cities, as all scenarios result in an energy loss for the DGW-SSPCM system compared to the DGW-REF system. This is due to the higher ambient temperatures under summer sunny conditions in Miami compared to Montreal and Vancouver. The energy loss for cases 1 to 9 compared to DGW-REF system are 12.2, 12.2, 12.2, 15.1, 14.0, 12.6, 5.0, 5.0, and 5.1 kJ, respectively. The lowest energy losses are observed in cases 7, 8, and 9, where the SSPCM remains transparent throughout the entire day.

Fig. 16 illustrates the thermal energy in all studied cases, under summer cloudy conditions in the three studied cities. In Miami and Montreal, the SSPCM-DGW system show energy losses in all cases, due to hot ambient temperatures in summer cloudy conditions and the absent of direct solar irradiation. In Montreal, the energy loss for cases 1 to 9 compared to DGW-REF system are 45.1, 45.1, 45.1, 48.4, 47.4, 45.4, 39.7, 39.7, 39.7, and 39.7 kJ, respectively. In Miami, the energy loss for cases 1 to 9 compared to DGW-REF system are 33.6, 33.6, 33.6, 36.3, 35.0, 33.3, 27.5, 27.5, and 27.5 kJ, respectively. For both cities, the lowest energy losses are attributed to the cases 7, 8, and 9 ($T_c = 30\ ^\circ C$), where the SSPCM remains transparent throughout the entire day. The system's behavior in Vancouver differs due to lower ambient temperatures during summer cloudy conditions compared to the other two cities. In Vancouver, the thermal energy values are positive, with lower values indicating energy savings by preventing the escape of air-conditioned air from the building. In Vancouver, the energy savings for cases 1 to 9 compared to DGW-REF system are 16.7, 16.9, 18.3, 23.2, 22.4, 21.6, 15.7, 15.7, and 15.7 kJ, respectively. The highest energy savings attributed to the cases 4, 5, and 6 in which the SSPCM undergoes a partial phase transition during the day. In addition, although among the three cases, case 4 with the lowest ΔT_c results in higher energy savings, the difference is not significant. It can be inferred that the impact of the SSPCM's T_c on the energy savings of the glazing system is more significant than the effect of its ΔT_c.

According to Figs. 15 and 16, in Vancouver, energy savings are obtained using the SSPCM-DGW system on both sunny and cloudy days. Hence, using this glazing system would enhance thermal energy performance in Vancouver during summer, while maintaining visual clarity. In Montreal, energy savings are achieved on sunny days, while energy losses occur on cloudy days. Comparing the amounts of energy saved and lost for the case with the highest energy saving, it is evident

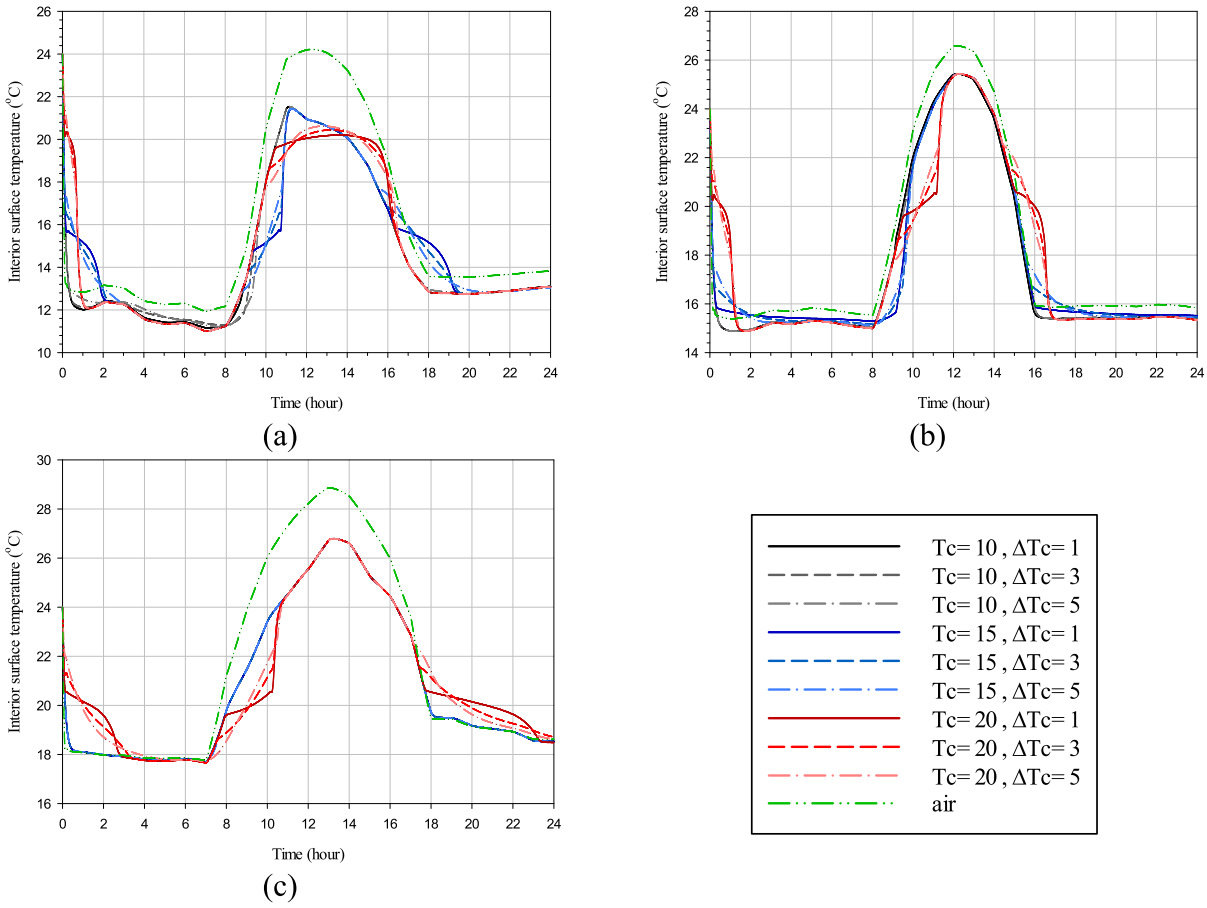

Fig.13. SSPCM's interior surface temperature variations in winter sunny conditions for (a) Montreal, (b) Vancouver, (c) and Miami.

that the energy lost on a cloudy day is more (almost 2.3 times) than the energy saved on a sunny day. In Miami, using the proposed SSPCM-DGW system results in energy losses during summer on both cloudy and sunny days. Therefore, having a 2 mm SSPCM attached to the inner pane of a DGW in Miami would not be beneficial in terms of energy savings.

Fig. 17 shows the thermal energy for all the cases studied under winter sunny conditions in the three cities analyzed. This figure indicates an energy loss in all cases under these conditions. The energy loss for cases 1 to 9 compared to the DGW-REF system are 87.4, 86.6, 85.2, 66.5, 66.3, 66.5, 64.4, 64.4, and 64.5 kJ for Montreal; 23.9, 23.9, 23.9, 18.7, 16.1, 15.5, 7.2, 7.1, and 7.1 kJ for Vancouver; and 71.8, 71.8, 71.8, 71.8, 71.8, 71.8, 61.4, 61.7, and 62.9 kJ for Miami. The energy losses across all cities under winter sunny conditions suggest that the blockage of direct solar irradiation during the day by the SSPCM has been greater than the heat released into the indoor environment at night, resulting in a net energy loss. The lowest energy loss is observed in cases 7, 8, and 9 ($T_c = 20$ °C), where the SSPCM undergoes a phase transition, releasing the heat stored during the day into the indoor environment at night, and also stays transparent for a longer period during the day. Furthermore, it is observable that although the effect of ΔT_c on the glazing energy performance is not significant, higher values result in less energy loss due to the SSPCM's longer charging and discharging times. It is also evident that energy losses in Vancouver are less than in the other two cities. The winter ambient temperature in Vancouver remains between those of the other two cities. This highlights the fact that designing an appropriate glazing system incorporating thermal energy storage materials needs to be considered case by case, due to the substantial number of dependent parameters affecting the energy performance and visual aspects of the fenestration system.

Under winter cloudy conditions, the behavior of the fenestration system differs, resulting in energy savings in all three cities, as shown in Fig. 18. In the absence of direct solar irradiation, the SSPCM not only releases the stored heat during the day into the indoor environment at night but also it acts as an insulator, retaining the warmed air within the building. The energy savings for cases 1 to 9 compared to the DGW-REF system are as follows: 10.9, 11.9, 13.7, 39.0, 39.1, 38.5, 39.3, 39.3, and 39.2 kJ for Montreal; 30.0, 30.0, 30.0, 37.2, 39.9, 40.4, 50.6, 50.6, and 50.5 kJ for Vancouver; and 42.8, 42.8, 42.8, 42.8, 42.8, 42.8, 54.9, 54.4, and 53.0 kJ for Miami. It is visible that the cases 7, 8, and 9 ($T_c = 20$ °C) yields the highest energy savings due to the phase transition of the SSPCM through the day. The highest energy savings are attributed to Miami, followed by Vancouver, and then Montreal. days. Comparing the amounts of energy saved and lost for the case with the highest energy saving, it is evident that in Montreal and Miami, the energy lost on a sunny day is almost 1.7 and 1.2 times, respectively, greater than the energy saved on a cloudy day. In contrast, in Vancouver, the energy saved on a cloudy day is almost 7.1 times greater than the energy lost on a sunny day. Consequently, the use of the proposed SSPCM-DGW in winter is undoubtedly beneficial in Vancouver in terms of energy savings.

5. Conclusion

This study focuses on evaluating the energy efficiency of a double-glazing system that integrates a solid–solid phase change material (SSPCM) with limited thickness, applied to the inner glass pane within the air gap. The SSPCM is preferred due to its superior properties compared to traditional liquid–solid phase change materials in glazing applications. Numerical simulations were conducted using a model developed with the finite volume method in ANSYS FLUENT. The

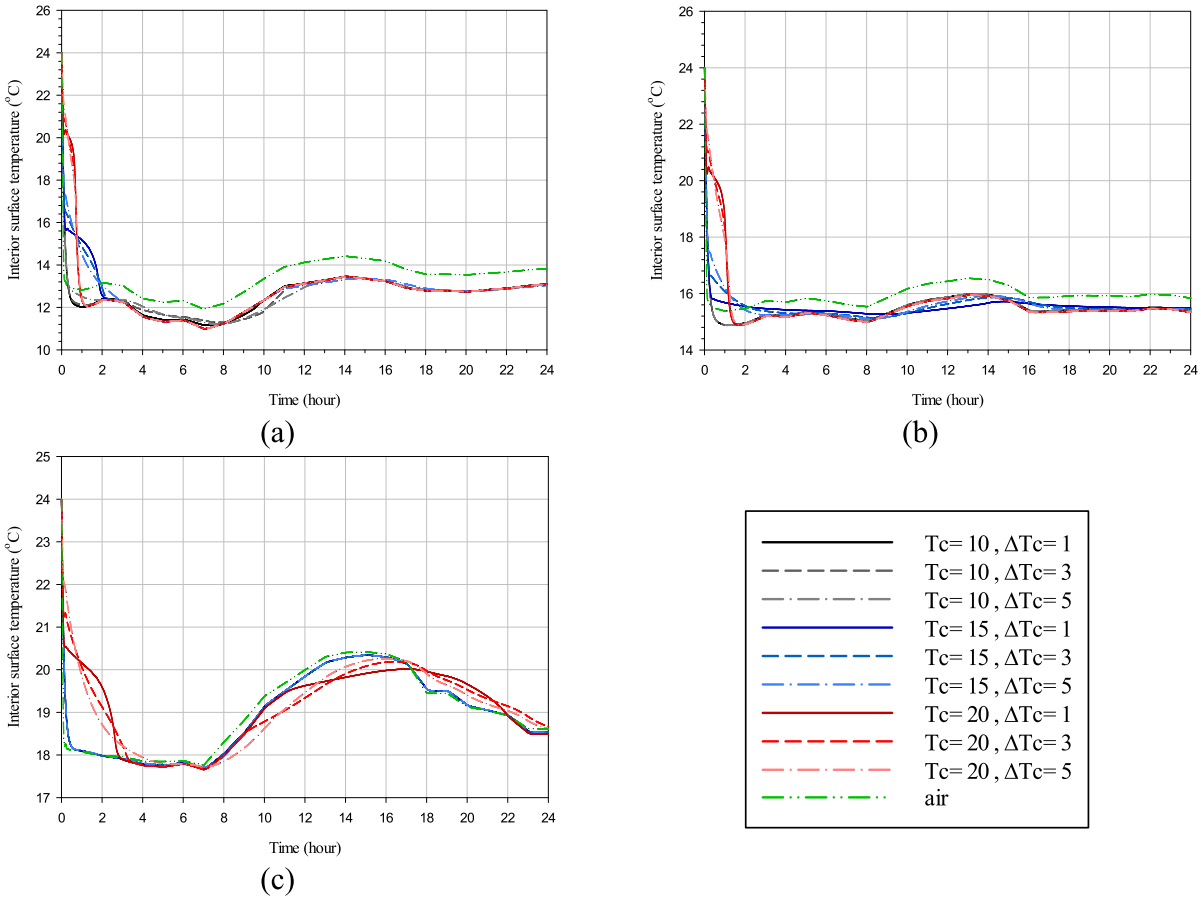

Fig.14. SSPCM's interior surface temperature variations in winter cloudy conditions for (a) Montreal, (b) Vancouver, (c) and Miami.

Table 6
Thermal energy values (in kJ) for all studied scenarios across the three cities.

Climatic condition	City	Case 0	Case 1	Case 2	Case 3	Case 4	Case 5	Case 6	Case 7	Case 8	Case 9
Summer sunny	Montreal	−99.7	−89.3	−89.3	−89.3	−93.7	−92.5	−90.2	−82.3	−82.3	−82.3
	Vancouver	−90.1	−72.7	−73.0	−74.4	−80.4	−79.2	−78.3	−69.0	−69.4	−69.6
	Miami	−93.2	−105.4	−105.4	−105.4	−108.3	−107.2	−105.8	−98.1	−98.1	−98.3
Summer cloudy	Montreal	−11.2	−56.2	−56.2	−56.2	−59.6	−58.5	−56.6	−50.9	−50.9	−50.9
	Vancouver	43.3	26.6	26.3	25.0	20.1	20.9	21.7	27.6	27.6	27.6
	Miami	−46.1	−79.6	−79.6	−79.6	−82.3	−81.0	−79.3	−73.6	−73.6	−73.6
Winter sunny	Montreal	342.1	429.6	428.8	427.3	408.6	408.4	408.7	406.5	406.6	406.6
	Vancouver	228.8	252.7	252.7	252.7	247.5	244.9	244.3	235.9	235.9	235.9
	Miami	–22.9	48.9	48.9	48.9	48.9	48.9	48.8	38.5	38.8	39.9
Winter cloudy	Montreal	559.0	548.1	547.1	545.3	519.9	519.9	520.5	519.7	519.7	519.8
	Vancouver	408.2	378.2	378.2	378.2	370.9	368.2	367.7	357.6	357.6	357.6
	Miami	209.6	166.8	166.8	166.8	166.8	166.8	166.7	154.7	155.2	156.6

accuracy of this model was confirmed by comparing its predictions with experimental data, which showed a high level of agreement. The model was then used to explore various transient temperature values and ranges within the proposed glazing system to determine its energy performance under both the coldest and hottest days of the year, as well as during cloudy and sunny days in Montreal (Dfb), Vancouver (Cfb), and Miami (Aw). A 2 mm thickness of SSPCM was utilized, with transient temperature values between 15 °C and 30 °C and transient temperature ranges between 1 °C and 5 °C. The findings reveal significant differences in energy savings across the three cities, emphasizing the importance of localized climate conditions in assessing the efficacy of energy-saving technologies. The obtained results are as follows:

- In Montreal under summer sunny conditions, the SSPCM-DGW system demonstrates consistent energy savings compared to the DGW-REF system. The most notable savings are achieved in cases where the SSPCM remains opaque throughout the day with T_c = 20 °C, although these configurations compromise visual clarity. Optimal results are observed in cases where the SSPCM remains transparent, balancing energy efficiency and visual clarity. However, under summer cloudy conditions, the system results in energy losses, with the energy lost on cloudy days being approximately 2.3 times greater than the energy saved on sunny days. The effect of transient temperature ranges of 1, 2, and 3 °C on thermal energy is subtle across all scenarios but becomes more pronounced when the SSPCM undergoes a phase transition at Tc = 25 °C.
- Vancouver shows a similar trend with energy savings in all scenarios under summer sunny conditions. Under these climatic conditions, the highest thermal energy savings for the DGW-SSPCM system are observed at Tc = 30 °C, averaging 20.5 kJ (23 %) for the three

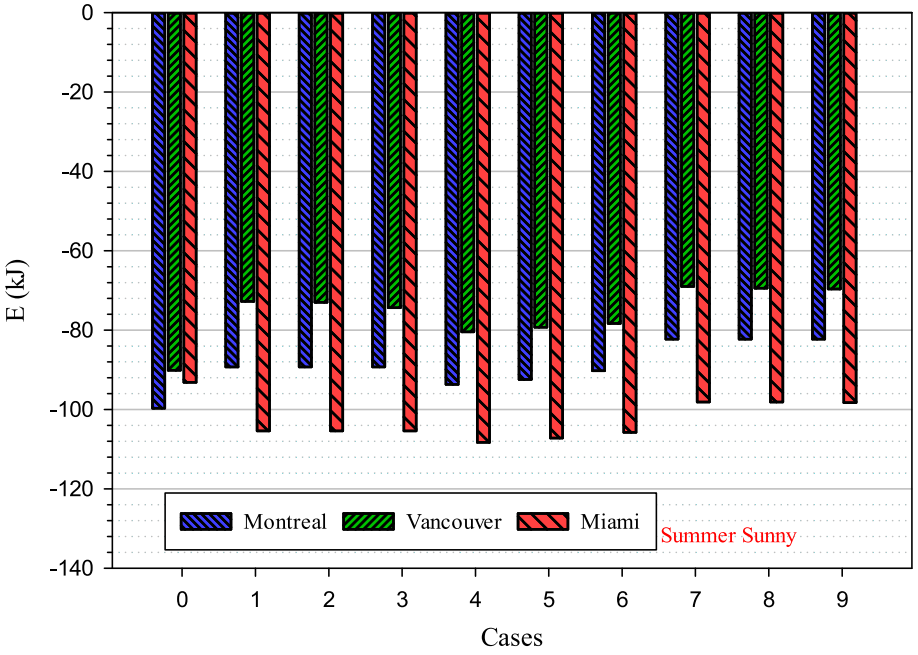

Fig.15. The thermal energy in all studied scenarios under summer sunny conditions in Montreal, Vancouver, and Miami.

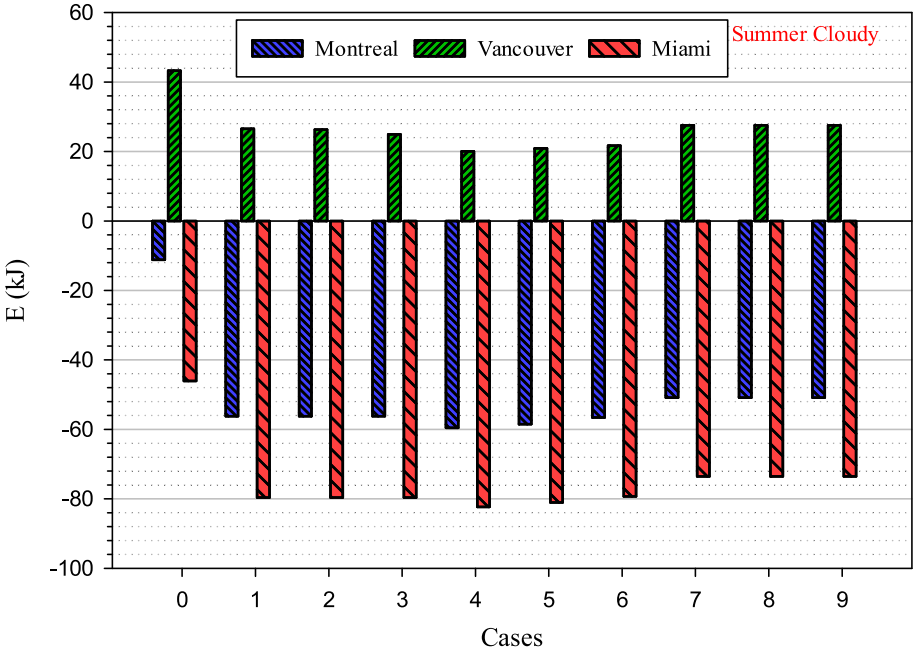

Fig.16. The thermal energy in all studied scenarios under summer cloudy conditions in Montreal, Vancouver, and Miami.

transient temperature ranges of 1, 2, and 3 °C in relation to the DGW-REF system. The energy performance is particularly enhanced under both sunny and cloudy days, making the SSPCM-DGW system highly beneficial for summer use while maintaining visual clarity. Under winter conditions, Vancouver benefits the most from the SSPCM-DGW system, with the energy saved on cloudy days (50.6 kJ) being almost 7.1 times greater than the energy lost on sunny days (7.1 kJ), highlighting the system's suitability for this city's moderate climate.

- In Miami, the SSPCM-DGW system results in energy losses by 60 % and 5 % (at T_c = 30 °C) under both summer sunny and cloudy conditions, respectively, due to the high ambient temperatures. The energy losses observed indicate that the SSPCM-DGW system is not suitable for Miami's climate during the summer.
- During winter sunny conditions, all three cities experience energy losses with the SSPCM-DGW system, as the blockage of direct solar irradiation by the SSPCM surpasses the heat released into the indoor environment at night. The lowest energy losses are observed in cases where the SSPCM undergoes a phase transition and remains transparent for a longer period during the day. Notably, Vancouver exhibits the lowest energy loss among the three cities of 7.1 kJ (3 %), which can be attributed to its moderate winter temperatures, while Montreal shows the highest energy loss of 64.4 kJ (19 %) at T_c = 30 °C.

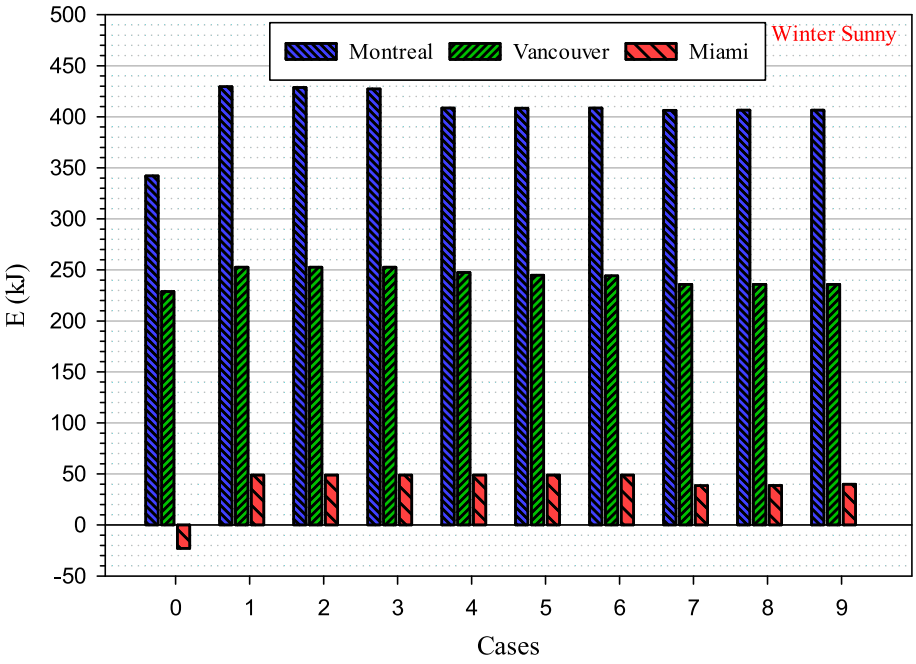

Fig.17. The thermal energy in all studied scenarios under winter sunny conditions in Montreal, Vancouver, and Miami.

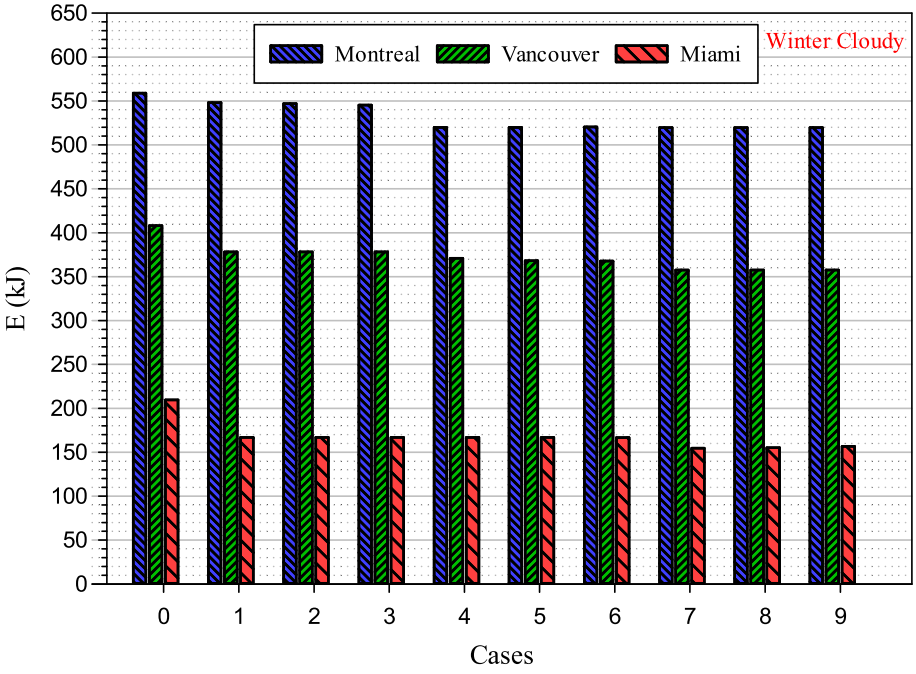

Fig.18. The thermal energy in all studied scenarios under winter cloudy conditions in Montreal, Vancouver, and Miami.

- Under winter cloudy conditions, the SSPCM-DGW system yields energy savings in all three cities by acting as an insulator and releasing stored heat at night. The highest energy savings are observed in Miami (54.5 kJ, 26 %), followed by Vancouver (50.6 kJ, 12 %), and Montreal (39.3 kJ, 7 %). In Montreal and Miami, the energy lost on a sunny day is significantly higher than the energy saved on a cloudy day, while in Vancouver, the energy saved on a cloudy day far exceeds the energy lost on a sunny day.
- In all cases, the transient temperature of the SSPCM has a more pronounced impact on the energy savings of the glazing system than the transient temperature range.

Lastly, the SSPCM-DGW system proves to be beneficial in Vancouver across various conditions in terms of energy performance. For Montreal and Miami, the system's effectiveness is limited due to the respective weather conditions that lead to higher energy losses. These results underscore the necessity of considering localized climate factors when designing and implementing energy-efficient glazing systems. Considering the significant importance of providing a proper visual view, the SSPCM-DGW system offers complete visual clarity during office hours when undergoing a full phase transition, making it more suitable for commercial buildings.

For future research directions, several tasks could be considered. First, conducting experimental studies to validate the use of SSPCMs in

glazing systems is crucial, particularly due to the current lack of experimental data in this domain. Additionally, simulating the system over consecutive days would provide a more comprehensive understanding of its long-term energy performance. Expanding the simulations to encompass various days throughout the year, coupled with the use of machine learning and optimization methods, could further refine the predictive modeling of the system's energy performance and optical properties across different climates and time periods. Furthermore, integrating ANSYS Fluent with EnergyPlus could enhance the accuracy of the simulations while reducing computational costs, enabling a more efficient evaluation of the system over extended periods. Last but not the least, conducting experimental studies to obtain more precise thermophysical and optical properties of SSPCMs would lead to more accurate modeling and optimization of these materials in building envelope applications, ultimately contributing to the development of more energy-efficient glazing systems.

CRediT authorship contribution statement

Hossein Arasteh: Writing – original draft, Validation, Software, Methodology, Investigation, Formal analysis, Data curation, Conceptualization. **Wahid Maref:** Writing – review & editing, Supervision, Project administration, Methodology, Conceptualization. **Hamed H. Saber:** Writing – review & editing, Visualization, Supervision, Software, Project administration, Conceptualization.

Declaration of competing interest

The authors declare that they have no known competing financial interests or personal relationships that could have appeared to influence the work reported in this paper.

Data availability

Data will be made available on request.

References

[1] S. Wang, T. Jiang, Y. Meng, R. Yang, G. Tan, and Y. Long, "Scalable thermochromic smart windows with passive radiative cooling regulation," *Science (1979)*, vol. 374, no. 6574, pp. 1501–1504, Dec. 2021, doi: 10.1126/science.abg0291.

[2] K. Cho, D. Cho, B. Koo, Y. Yun, Thermal Performance Analysis of Windows, Based on Argon Gas Percentages between Window Glasses, Buildings 13 (12) (2023) 2935.

[3] F. Chen, X. Wu, G. Lu, J. Nie, X. Zhu, Thermochromic Hydrogels with Adjustable Transition Behavior for Smart Windows, ACS Appl Mater Interfaces 16 (16) (2024) 21013–21023.

[4] A.K. Mohammad, A. Ghosh, Exploring energy consumption for less energy-hungry building in UK using advanced aerogel window, Solar Energy 253 (2023) 389–400.

[5] M.M. Uddin, J. Ji, C. Wang, C. Zhang, Building energy conservation potentials of semi-transparent CdTe integrated photovoltaic window systems in Bangladesh context, Renew Energy 207 (2023) 512–530.

[6] D. Wang, G. Chen, J. Fu, Multifunctional thermochromic smart windows for building energy saving, J Mater Chem A Mater (2024).

[7] H. Liu, W. He, X. Liu, J. Zhu, H. Yu, Z. Hu, Building integrated concentrating photovoltaic window coupling luminescent solar concentrator and thermotropic material, Energy 284 (2023) 129237.

[8] M. Han, J. Pu, Y. Liu, X. Liu, H. Mei, C. Shen, Near-infrared blocking window based on ATO-CWO/PVB nano-lamination, Renew Energy 219 (2023) 119382.

[9] E. Sorooshnia, et al., A novel approach for optimized design of low-E windows and visual comfort for residential spaces, Energy and Built Environment (2023).

[10] E. Field, A. Ghosh, Energy assessment of advanced and switchable windows for less energy-hungry buildings in the UK, Energy 283 (2023) 128999.

[11] H. Arasteh, W. Maref, H.H. Saber, Energy and thermal performance analysis of PCM-Incorporated glazing units combined with passive and active techniques: A review study, Energies (basel) 16 (3) (2023) 1058.

[12] A. Fallahi, G. Guldentops, M. Tao, S. Granados-Focil, S. Van Dessel, Review on solid-solid phase change materials for thermal energy storage: Molecular structure and thermal properties, Appl Therm Eng 127 (2017) 1427–1441.

[13] Y. Gao, et al., Parametric study of solid-solid translucent phase change materials in building windows, Appl Energy 301 (2021) 117467.

[14] P. Wang, Z. Liu, L. Zhang, Z. Wang, J. Fan, Inversion of extinction coefficient and refractive index of variable transparency solid–solid phase change material based on a hybrid model under real climatic conditions, Appl Energy 341 (2023) 121098.

[15] C.R. Raj, S. Suresh, R.R. Bhavsar, V.K. Singh, Recent developments in thermo-physical property enhancement and applications of solid solid phase change materials: A review, J Therm Anal Calorim 139 (2020) 3023–3049.

[16] G. Guldentops, G. Ardito, M. Tao, S. Granados-Focil, S. Van Dessel, A numerical study of adaptive building enclosure systems using solid–solid phase change materials with variable transparency, Energy Build 167 (2018) 240–252.

[17] Y. Ma, et al., Energy and daylighting performance of a building containing an innovative glazing window with solid-solid phase change material and silica aerogel integration, Energy Convers Manag 271 (2022) 116341.

[18] C. Zhang, et al., Parametric research on thermal and optical properties of solid-solid phase change material packaged in glazing windows, J Energy Storage 83 (2024) 110562, https://doi.org/10.1016/j.est.2024.110562.

[19] ASHRAE. ASHRAE Handbook of Fundamental, Effective Thermal Resistance of Plane Air Spaces; Chapter 26, Table 3; ASHRAE: Peachtree Corners, Georgia, 2021; pp. 26.14–26.15.

[20] B.L. Gowreesunker, S.B. Stankovic, S.A. Tassou, P.A. Kyriacou, Experimental and numerical investigations of the optical and thermal aspects of a PCM-glazed unit, Energy Build 61 (2013) 239–249.

[21] Available online: https://www.pcmproducts.net/Phase_Change_Material_Products.htm, (accessed on 17 October 2023).

[22] A.N.S.Y.S. Ansys, Fluent; Ver., R1; ANSYS FLUENT: Canonsburg, PA, USA, 2022, p. 2022.

[23] A.D. Brent, V.R. Voller, K. t J. Reid, Enthalpy-porosity technique for modeling convection-diffusion phase change: application to the melting of a pure metal, Numeri Heat Transf A Appl 13 (3) (1988) 297–318.

[24] A.W.J. Heijs, C.P. Lowe, Numerical evaluation of the permeability and the Kozeny constant for two types of porous media, Phys Rev E 51 (5) (1995) 4346.

[25] H.E. Beck, N.E. Zimmermann, T.R. McVicar, N. Vergopolan, A. Berg, E.F. Wood, Present and future Köppen-Geiger climate classification maps at 1-km resolution, Sci Data 5 (1) (2018) 1–12.

[26] Available online: https://weatherspark.com/h/d/18622/2022/1/30/Historical-Weather-on-Sunday-January-30-2022-in-Miami-Florida-United-States#Figures-Temperature (accessed on 4 December 2023).

[27] Available online: https://climate.weather.gc.ca (accessed on 18 December 2023).

[28] G. A. S. of H. R. and A. C. Engineers. Peachtree Corners, "Effective Thermal Resistance of plane Air Spaces.", in ASHRAE ASHRAE handbook of fundamental ch. 26 2021 pp. 26.14-26.14.

[29] Ministry of Housing and Urban-Rural Development of the People's Republic of China, Code for thermal design of civil building, China Architecture & Building Press, Beijing, 2016.

[30] H.H. Saber, W. Maref, A.E. Hajiah, Hygrothermal performance of cool roofs subjected to Saudi climates, Front Energy Res 7 (2019) 39.

[31] F. Goia, M. Perino, M. Haase, A numerical model to evaluate the thermal behaviour of PCM glazing system configurations, Energy Build 54 (2012) 141–153.